Differential subclass pathogenicity of antibodies in a mouse model of pulmonary vasculitis

Dissertation

der Fakultät für Biologie

der Ludwig-Maximilians-Universität München

Stefanie Anne Weiß

München, den 28. April 2020

Diese Dissertation wurde angefertigt
unter der Leitung von **PD Dr. Dieter Jenne**
am **Helmholtz Zentrum München**
Deutsches Forschungszentrum für Gesundheit und Umwelt
Comprehensive Pneumology Center

Erstgutachterin:	Prof. Dr. Elisabeth Weiß
Zweitgutachter:	Prof. Dr. Christof Osman
Tag der Abgabe:	28.04.2020
Tag der mündlichen Prüfung:	12.01.2021

TABLE OF CONTENTS

Summary

Anti-neutrophil cytoplasm antibodies (ANCA) against proteinase 3 (PR3) and myeloperoxidase (MPO) are found in 80% of patients with autoimmune vasculitides. Anti-PR3 autoantibodies are found in granulomatosis with polyangiitis (GPA), anti-MPO-ANCA in eosinophilic GPA (EGPA) and microscopic polyangiitis (MPA), which are all characterized by inflammation of the microvasculature. The predominantly affected organs are the respiratory tract and the kidneys. In view of initial observations in a mouse model of anti-PR3 associated pulmonary vasculitis, we hypothesized that the murine subclass IgG2, especially IgG2c, has a major pathogenic effect.

To analyze this subclass-specific effect of anti-PR3 antibodies, we sequenced the heavy and light chains of two hybridoma-derived monoclonal antibodies against human PR3. The epitope-specific variable regions were fused to constant domains of murine IgG1 and IgG2c subclasses resulting in two sets of epitope-matched monoclonal anti-hPR3 antibodies in single-chain as well as native occurring two-chain format. The same methods were applied for the production of two-chain antibodies against murine MPO as IgG1 and IgG2c subclasses.

In this study, I present *in vivo* data showing that systemic application of recombinant anti-MPO IgG2c caused a vasculitis-like phenotype with hemorrhages and inflammation in the lungs of mice, while the epitope-matched recombinant IgG1 antibodies had no effect in this experimental pulmonary model. These findings indicate a crucial effect of subclass-specific antibody pathogenicity in mice and suggest a potential similar mechanism in humans.

Zusammenfassung

Anti-neutrophile cytoplasmische Antikörper (ANCA) gegen Proteinase 3 (PR3) und Myeloperoxidase (MPO) treten in 80% der Patienten mit Autoimmunvaskulitis auf. Anti-PR3-Autoantikörper finden sich bei Granulomatose mit Polyangiitis (GPA), anti-MPO-ANCA bei eosinophiler GPA (EGPA) und mikroskopischer Polyangiitis (MPA), die alle durch eine Entzündung der Mikrovaskulatur gekennzeichnet sind. Überwiegend betroffene Organe sind die Atemwege und die Nieren. Angesichts erster Beobachtungen in einem Mausmodell der anti-PR3-assoziierten pulmonalen Vaskulitis stellten wir die Hypothese auf, dass die murine Subklasse IgG2, insbesondere IgG2c, eine bedeutende pathogene Wirkung hat.

Um diesen subklassenspezifischen Effekt der anti-PR3 Antikörper zu analysieren, sequenzierten wir die schweren und leichten Ketten zweier vom Hybridom abgeleiteter monoklonaler Antikörper gegen humane PR3. Die Epitop-spezifischen variablen Regionen wurden mit konstanten Domänen der murinen IgG1- und IgG2c-Subklassen fusioniert, wodurch zwei Sätze Epitop-angepasster monoklonaler anti-hPR3 Antikörper sowohl im Einzelketten- als auch im nativ vorkommenden Zweikettenformat entstanden. Desweiteren wurden Zwei-Ketten-Antikörper gegen murine MPO als IgG1- und IgG2c-Subklassen mit der gleichen Methodik produziert.

In dieser Studie präsentiere ich *in vivo* Daten, die zeigen, dass die systemische Applikation von rekombinantem anti-MPO-IgG2c einen vaskulitis-ähnlichen Phänotyp mit Blutungen und Entzündungen in den Lungen von Mäusen verursachte, während die Epitop-angepassten rekombinanten IgG1-Antikörper in diesem experimentellen Lungenmodell keine Wirkung zeigte. Diese Befunde weisen auf einen entscheidenden Effekt der subklassenspezifischen Pathogenität von anti-MPO Antikörpern bei Mäusen hin und deuten auf einen möglicherweise ähnlichen Mechanismus beim Menschen hin.

1. Introduction

1.1 Classification of systemic vasculitides

Vasculitides form an extraordinarily heterogeneous group of inflammatory vascular diseases, which manifest clinically in many different ways. The inflammatory process can affect almost all blood vessels and therefore have an impact on a variety of organs. According to the 2012 revised international Chapel Hill consensus conference nomenclature of vasculitides, the classification of vasculitides is mainly based on the size of the primarily affected vessels: large, medium, and small (Figure 1) (Jennette et al., 2013).

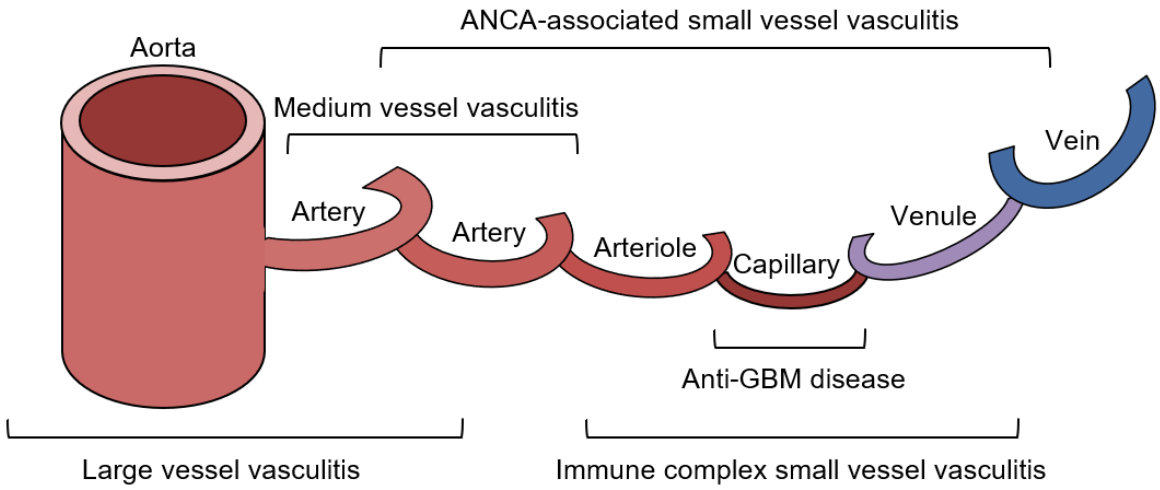

Figure 1: Classification of systemic vasculitides according to the size of the affected vessels. ANCA (anti-neutrophil cytoplasm antibody), GBM (glomerular basement membrane). Adapted from (Jennette et al., 2013).

1.1.1 ANCA-associated vasculitis

A subgroup of small-vessel vasculitis is strongly associated with the presence of anti-neutrophil cytoplasm antibodies (ANCA) and is therefore called ANCA-associated vasculitis (AAV). Based on the clinical manifestations AAV can be further classified into three entities:

Granulomatosis with polyangiitis (GPA), eosinophilic granulomatosis with polyangiitis (EGPA), and microscopic polyangiitis (MPA) (Jennette et al., 2013). All three subtypes are so-called pauci-immune autoimmune vasculitides, because no or only very few immune complexes and complement deposits can be detected in the affected tissues.

With an annual incidence rate of around 20 per million in Europe and North America, AAV occurs worldwide in different populations (Ntatsaki et al., 2010). AAV, however, is more common in white and Asian populations and less common in African American populations (Watts et al., 2015). It generally occurs more frequently in men than in women (Watts et al., 2000).

If untreated, AAV has a two-year mortality rate of 93%, primarily due to respiratory and renal failure (Frohnert and Sheps, 1967). The induction and application of immunosuppressive drugs such as glucocorticoids and cyclophosphamide since the 1950s, has improved the survival of AAV patients to 75% within the first 10 years after the initial treatment (Flossmann et al., 2011). This therapeutic revolution has converted AAV into a relapsing and remitting disease with progressive organ damage in the majority of patients.

1.1.2 Granulomatosis with polyangiitis

The annual incidence rate of GPA, which is also known as Wegener´s granulomatosis, lies between 2.4 and 14.4 cases per million in Europe and the initial diagnosis is often made in patients aged 40 to 60 years, but cases have also been described in younger people and adolescents (Hilhorst et al., 2015). Men and women are equally affected by this disease which usually progresses in two phases: First, granulomatous lesions appear in the upper respiratory tract (Hartl et al., 1998). Within a few weeks, or often after months or years, the transition to the generalized form occurs in most cases, which is usually characterized by vasculitis of the small arteries, capillaries and veins (Hoffman et al., 1992). However, organ involvement is extremely variable: the disease preferentially manifests in the nose and sinuses, followed by the lungs and kidneys. Less frequently, the heart, liver, joints, eyes, skin, nervous system,

trachea, and the gastrointestinal tract are affected (Fauci et al., 1994). Typically, vasculitis, granuloma formation in the lungs, and segmental necrotizing glomerulonephritis occur (Aasarød et al., 2000). The main hallmark and diagnostic marker of GPA is the presence of ANCA directed against proteinase 3 (PR3) in 75% of the patients at initial presentation (Drooger et al., 2009). Furthermore, infections have an impact on the progress of GPA. 60% to 70% of patients are chronically carrying *Staphylococcus aureus* which increases the risk for relapses (Stegeman et al., 1994).

1.1.3 Eosinophilic granulomatosis with polyangiitis

In contrast to GPA the autoantibodies detected in patients suffering from EGPA, formerly called Churg-Strauss-Syndrome, are predominantly directed against myeloperoxidase (MPO), although they are only present in 40% of patients (Sable-Fourtassou et al., 2005). With an incidence rate of 1-4 per million inhabitants per year, EGPA is less common than GPA (Berti et al., 2017; Mahr et al., 2014) Even though the average age at initial diagnosis is 50 years, the disease can already occur at a young age (Gioffredi et al., 2014). Women are affected more than men. In contrast to GPA, EGPA proceeds in three phases, the occurrence and sequence of which greatly varies between patients (Lanham et al., 1984; Sinico et al., 2005). The prodromal stage is characterized by allergy and more than 90% of EGPA patients are diagnosed with asthma before diagnosis or within the disease course. In the second stage, hyper eosinophilia occurs in the blood of patients and eosinophils are infiltrating into organ tissues, predominantly of the lung and the digestive tract. The third vasculitic phase usually develops within 3 years after the beginning of the disease and is hallmarked by inflammation of blood vessels and involvement of multiple organs. According to the American College of Rheumatology (ACR), EGPA can be diagnosed when four of the following six characteristics are present in addition to the signs of vasculitis: asthma, eosinophilia, neuropathy, lung infiltrates, sinus abnormalities and eosinophilic vasculitis (Fries et al., 1990).

1.1.4 Microscopic polyangiitis

MPA is mainly hallmarked by the occurrence of antibodies against MPO in 60% of patients (Katsuyama et al., 2014). The clinical manifestations are similar to those of GPA, except that granulomatous destructive lesions are absent and the upper respiratory tract is usually only minimally affected or not affected at all.

1.2 Anti-neutrophil cytoplasmic antibodies

Autoantibodies associated with AAV were first reported in 1982 in the serum of a patient with segmental necrotizing glomerulonephritis (Davies et al., 1982). ANCA are predominantly directed against proteins localized in primary or azurophilic granules of neutrophils. Based on the immunofluorescence pattern on ethanol-fixed neutrophils, a distinction is made between c (=cytoplasmic) -ANCA and p (=perinuclear) -ANCA. C-ANCA are directed against the serine protease proteinase 3 (PR3) and occur in patients suffering from GPA (van der Woude et al., 1985) while p-ANCA bind to myeloperoxidase (MPO) and are associated with MPA and EGPA (Falk and Jennette, 1988). Even though ANCA are most strongly associated with AAV, they were also found in patients with various rheumatic autoimmune diseases such as systemic lupus erythematosus and rheumatoid arthritis (Merkel et al., 1997). However, the main significance of ANCA pathogenicity is connected to AAV. For a long time, the differential diagnosis of the three clinical entities was based on immunofluorescence staining. At present ELISA is initially performed on blood samples of the patients to detect ANCA as reliable biomarker (Jennette et al., 1998; Hagen et al., 1998).

Even though the value of ANCA at initial diagnosis is highly recognized, controversial views about their relevance in monitoring disease activity and relapses exist. Some studies demonstrated that ANCA titers correlated with disease activity (Vega and Espinoza, 2016), others reported that no relationship between ANCA levels and disease activity existed in patients (Rutgers et al., 2003). Although differences in pathogenicity of specific IgG subclasses

have been addressed, observational and functional analyses of ANCA subsets from AAV patients show pathogenic potential of ANCA across all human IgG subclasses (Colman et al., 2007). A better understanding of the sequence and structure of ANCA is necessary to improve the prediction of relapses and the therapeutic strategies in individual patients.

1.2.1 The role of ANCA in AAV pathogenesis

Neutrophils also play a general role in AAV like in all other inflammatory diseases, not only because the target antigens of ANCA are present in neutrophils. The interaction of ANCA with neutrophils, in particular however, leads to the induction of important cellular responses resulting in highly inflammatory vascular damage. In order to initiate signaling events with subsequent neutrophil activation the target antigens, PR3 or MPO, have to be accessible for recognition and binding by ANCA on the surface of neutrophils. MPO and the vast majority of PR3 are located in primary and azurophilic granules, which can be mobilized upon activation of neutrophils (Sengelov et al., 1995). In contrast to MPO, significant PR3 amounts are already expressed on the surface, while MPO is not detected on the plasma membrane of resting neutrophils (Halbwachs-Mecarelli et al., 1995). Upon activation, membrane expression is strongly increased, although to a lesser extent for MPO than PR3. The amount of membrane PR3 expressed on resting neutrophils differs between individuals, but the expression pattern is highly stable in a given person (Halbwachs-Mecarelli et al., 1995).

Quite often, the clinical onset of ANCA vasculitis is preceded by an infection of the upper respiratory tract (Ono et al., 2019). The resulting production of pro-inflammatory cytokines, like interleukins and tumor necrosis factor (TNF)-α, leads to a priming of neutrophils and antigen translocation. The binding of ANCA to the surface antigens on neutrophils then initiates signaling and full activation.

1.2.2 *In vitro* evidence

Neutrophil activation results in several processes like the release of reactive oxygen species (ROS), secretion of proteolytic enzymes and pro-inflammatory cytokines, and formation of neutrophil extracellular traps (NETs) (Kettritz, 2012; Kessenbrock et al., 2009). Several studies showed that sera and purified ANCA from AAV patients were able to induce an oxidative burst in healthy human neutrophils, pretreated with TNF-α or IL-18 (Falk et al., 1990; Hewins et al., 2006). Furthermore, neutrophil serine proteases (NSPs) released from ANCA-activated neutrophils were reported to cleave extracellular matrix proteins and to damage vascular endothelial cells (Ewert et al., 1992; Lu et al., 2006). Besides this direct effect on the cellular environment, pro-inflammatory cytokines indirectly contribute to the progress of the disease by attracting and priming even more neutrophils and other immune cells to the site of injury. This inflammatory loop ultimately results in small-vessel vasculitis.

1.2.3 *In vivo* evidence

The so far best evidence of ANCA pathogenicity *in vivo* was provided by the group of JC Jennette in 2002. The model they used is based on polyclonal anti-MPO antibodies which were isolated as total IgGs from MPO-deficient mice after immunization with murine MPO. Intravenous injection of splenocytes from these mice to mice deficient in recombinase-activating gene-2 (Rag2-/- mice), which are lacking mature B- and T- lymphocytes, induced a dose-dependent elevation of anti-MPO IgG titers. Human symptoms of AAV like hematuria, proteinuria and leukocyturia could be observed. Additionally, the kidneys of the mice showed extensive focal necrotizing glomerulonephritis with crescent formation and necrosis in 80% of glomeruli. Vascular inflammation was also found in other organs like the lungs, spleen, and lymph nodes (Xiao et al., 2002). The drawback of this experimental ANCA model is the limited purity of the immunogen which was isolated from a murine macrophage cell line WEHI and the use of Freund´s complete adjuvant. The polyclonal responses to MPO, to the adjuvants and to the contaminating proteins inducing the disease altogether are not well defined.

The transferred splenocyte population harbors many different B-cell clones, producing a polyclonal set of IgG with different subclasses and epitope specificities. More recently, the first *in vivo* model of vasculitis using monoclonal antibodies (mAbs) against MPO was established by Viehmann et al.. After an infectious trigger in the lungs of mice using LPS and fMLP and simultaneous application of a set of two anti-MPO mAbs, both of the IgG2 subclass, mice were developing a vasculitis-like phenotype in the lungs with severe inflammation and hemorrhages (unpublished data, Viehmann et al.).

The described model of anti-MPO induced pulmonary vasculitis is based on a similar model which was established for the investigation of human anti-PR3 ANCA in transgenic mice that express human instead of murine PR3 under the same genetic locus. MAbs towards hPR3 showed differential pathogenicity depending on the subclass identity. While for anti-hPR3 clone 4B12 (IgG2c) immune cell infiltration and inflammation in the lung could be observed, the clones 5B11 (IgG1) and 7D12 (IgG2b) showed no pathogenic potential. These preliminary observations could, however, not be reproduced (unpublished data, Hinkofer et al.).

Interaction of the neutrophil-specific receptor CD177 with PR3 on the membrane of resting neutrophils facilitates their activation after ANCA binding in humans. The CD177 binding site on mouse PR3 is missing and PR3 is not found on resting neutrophils in mice. This may explain why appropriate models for PR3-associated vasculitis are not yet available (Korkmaz et al., 2008). Attempts to establish a mouse model in double transgenic mice expressing both human PR3 and human CD177 failed to establish a disease phenotype *in vivo* (Schreiber et al., 2016).

1.3 Immunoglobulin G

Immunoglobulin G (IgG) is the most abundant isotype of immunoglobulins followed by IgA, IgM, IgD and IgE and accounts for 10-20% of protein in human plasma (Janeway, 2002). It is further divided into the four subclasses IgG1, IgG2, IgG3 and IgG4 (Schur, 1988). In mice three IgG subclasses, IgG1, IgG2 and IgG3 exist, and IgG2 is further subdivided into IgG2a, IgG2b

and IgG2c. While all mice are expressing IgG2b in their antibody repertoire, IgG2a and IgG2c are allelic and depending on the strain, mice are producing either IgG2a or IgG2c antibodies, in rare cases even both of them (Zhang et al., 2012). The most commonly used strain for *in vivo* studies of AAV, C57BL/6, for example is homozygous for the IgG2c allele.

In general, IgG2 consisting of IgG2a, IgG2b and IgG2c is the predominant murine subclass involved in pro-inflammatory processes (Weber et al., 2014), while in humans IgG1 and IgG3 antibodies of contribute most to inflammation (Nimmerjahn and Ravetch, 2006). On base of IgG structures and properties IgG, murine IgG2a/c is considered to be the functional equivalent of human IgG1, while murine IgG1 is similar to human IgG4.

Apart from the subclass differences in humans and mice, the general structure of IgG molecules is nevertheless well conserved between the two species. Two identical γ (gamma) heavy chains and two identical light chains are linked by inter-chain disulfide bonds to assemble a large Y-shaped protein with a molecular weight of about 150 kDa (Figure 2A). The heavy chain consists of an N-terminal variable region (V_H) and three constant regions (C_H1, C_H2, C_H3) which determine the subclass of the IgG molecule. A hinge region between C_H1 and C_H2 carries cysteines linking the two heavy chains of the IgG. The hinge is highly flexible and enables crosslinking of antigens by the two antigen binding sites of the IgG (Roux et al., 1997). The light chain similarly consists of a variable region (V_L) at the N-terminus but has only one constant region (C_L). Light and heavy chains are joined by one disulfide bond between C_H1 and C_L.

Although the overall amino acid sequences of the variable regions are similar in different antibodies three internal segments, the so-called complementary determining regions (CDRs) are highly variable and determine the antigen specificity of individual antibodies (Kabat et al., 1978). The diversity of antibodies arises from VDJ recombination, somatic mutations in the CDR regions of the V gene, and class switch recombination during the maturation of antibody-generating B-lymphocytes (Lieber, 2000; Li et al., 2004).

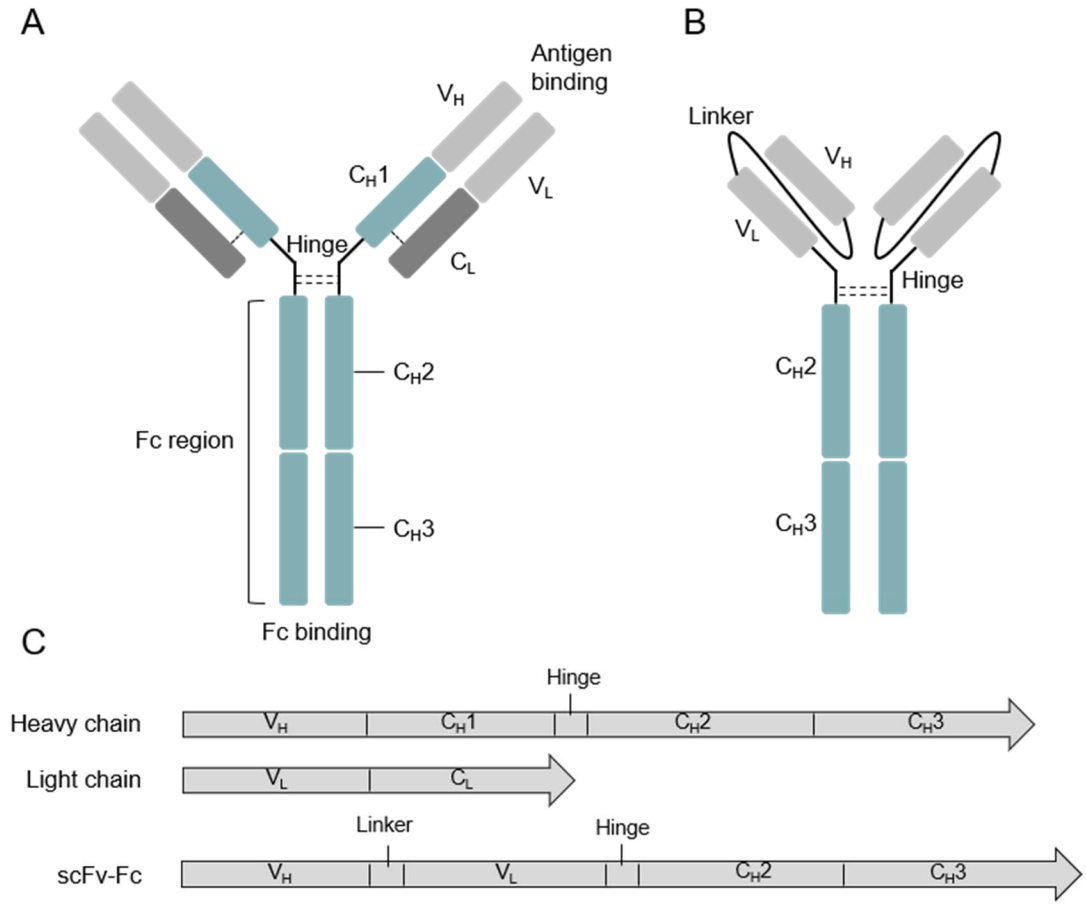

Figure 2: Structures of soluble Immunoglobulin G (A) and the adapted single chain format (scFv-Fc) used in this study (B). The variable regions (V_H and V_L) which determine antigen specificity are shown in light grey, the constant regions (C_H and C_L) of light chains are colored dark grey. Constant regions of the heavy chain (C_H1, C_H2 and C_H3) which determine the IgG subclass are highlighted in blue. Fc (crystallizable fragment). **(C)** The arrows show respective cDNA constructs for the recombinant production of two-chain IgG and scFv-Fc single chain antibodies.

In contrast to the specificity towards the antigen, the affinity and specificity to interact with Fc gamma receptors (FcγRs) is determined by the constant regions, mainly by that of the heavy chain (Bruhns, 2012). Consequently, IgGs of different subclasses have dissimilar potentials to interact with different FcγRs. All IgG molecules contain a conserved glycan at position N297 in the constant region of the heavy chains (Zauner et al., 2013). Many different IgG-Fc glycoforms exist but the core structure of the IgG glycans always comprises N-acetylglucosamine (GlcNAc) and mannose residues. Extendings of these glycans are variable

and the the final composition of the N297 glycan has an influence on the quaternary structure of the Fc and thus also an impact on the interaction with FcγRs (Bowden et al., 2012).

IgG antibodies are not only key players of the immune system but are used as important tools for research, diagnostics und therapeutic treatment. To date around 100 monoclonal antibodies (mAbs) are approved as drugs for the treatment of a variety of diseases including several types of cancer, inflammatory and autoimmune diseases (Kaplon et al., 2020). The most prominent example in context with vasculitis is the mAb rituximab which is used successfully in the treatment of GPA (Cornec et al., 2018). The V region of rituximab is directed against the surface receptor CD20 and induces selective cell depletion of CD20-positive B-cell subpopulations via Fc-mediated activation of effector cells. For this reason, the application of rituximab is also referred to as B-cell therapy (Reff et al., 1994).

Besides mAbs from hybridoma cell lines displaying the natural IgG structure, other recombinant formats of mAbs have been used and tailored for specific therapeutic applications. The single-chain variable fragment fused to the constant fragment (scFv-Fc) format (Figure 2B) allows to characterize candidate scFvs isolated from phage display libraries, which are commonly used to screen antibody repertoires. The advantages over the phage display-derived scFv, include a longer half-life, and Fc-mediated effector functions. This method facilitates the rapid screening of candidate antibodies, prior to a more time-consuming conversion into a full IgG format. While two cDNA constructs for the heavy chain and the light chains are needed for the recombinant production of two-chain antibodies, the scFv-Fc antibodies can be produced with only one cDNA construct (Figure 2C).

1.4 Fc gamma receptors

FcγRs are, like all FcRs, the crucial mediators of antibody-triggered responses and effector cell activation, linking innate and adaptive immune responses. The family of FcγRs consists of six members in humans, and to date four classes of FcγRs are known in mice (Nimmerjahn et al., 2005; Bruhns and Jönsson, 2015). They can be distinguished by their affinity for IgG subclasses and by the signaling pathways they induce (Bruhns et al., 2009). There is one high-affinity receptor, FcγRI in humans and mice, all other FcRs have low to medium affinity for the antibody Fc fragment (Su et al., 2002).

Except of FcγRIIB which has inhibitory properties through its cytoplasmic immunoreceptor tyrosine based inhibitory motif (ITIM) (Daëron et al., 2008), all members of FcγR act in an activating manner. Like the inhibitory FcγRIIB the human FcγRII class receptors FcγRIIA and FcγRIIC consist of a single ligand-binding α-chain. All other receptors of the Fcγ family carry an additional signal-transducing γ-chain, containing an immunoreceptor tyrosine based activating motif (ITAM) in their cytoplasmic part (Ra et al., 1989; Reth, 1989). In addition, humans have the glycosylphosphatidylinositol (GPI)-linked receptor called FcγRIIIB which is exclusively expressed by neutrophils (Scallon et al., 1989). FcγRIIIA instead is widely expressed on most leukocytes (Nimmerjahn and Ravetch, 2006). In general, a variety of human FcγR alleles with different functionality exist (Warmerdam et al., 1990; Ravetch and Perussia, 1989). For example, FcγRIIA^{131H} and the FcγRIIIA^{158V} have higher affinities for certain IgG subclasses compared to their allelic counterparts. It was shown that these polymorphisms play a role in AAV since patients homozygous for the respective alleles show a significantly faster time to progression and a faster positive response to immunosuppressive treatment with Rituximab (Robledo et al., 2012; Cartin-Ceba et al., 2017).

According to the genetic locus as well as molecular properties and the expression pattern on immune cells, the murine homologue to human FcγRIIIA is FcγRIV (Mechetina et al., 2002, Nimmerjahn et al., 2005). Surface plasmon resonance (SPR) analysis showed that murine

IgG2a and IgG2b can bind with high affinity to FcγRIV (association constants (K_A) of $2,7x10^7$ and $1,9x10^7$, respectively) while for IgG1 and IgG3 binding was not detected (Nimmerjahn et al., 2005). FcγRIV has therefore a distinct IgG subclass specificity. The binding affinity of the third variant of IgG2, namely IgG2c, has not been investigated by SPR. In view of the high structural similarities between the different IgG2 variants, however, it is reasonable to assume that the K_A towards FcγRIV is comparable to that of IgG2a and IgG2b.

1.5 Subclass specificities of ANCA

ANCA are predominantly of the IgG isotype and are found in all four human IgG subclasses. Several studies focused on the importance of IgG subclasses in AAV. Mulder et al. (1995) analyzed subsets of patients with GPA in different stages of disease and reported that IgG3 is more prominent and more pathogenic than the other subclasses, especially in patients with active disease. Similar studies by other groups also support the role of IgG3 as the main subclass contributing to ANCA pathogenicity (Colman et al., 2007). These data, however, are in conflict with other reports suggesting that IgG1 and IgG4 subclasses dominate both in GPA and MPA patients with ANCA against PR3 and MPO, respectively (Brouwer et al., 1991; Mellbye et al., 1994). Given the current state of research, it remains to be determined which ANCA subclasses predominate during active disease and have the highest pathogenicity. The differential role of ANCA subclasses in AAV is most likely due to their interaction with Fcγ and signaling through these receptors. Knowledge about their differential pathogenicity would open new opportunities for the treatment of individual AAV patients in different stages of disease.

1.6 Aim of the study

Even though ANCA pathogenicity has been extensively studied over the past decades it is still unclear whether antigen accessibility and epitope specificity or the subclass-dependent constant region matters for the pathogenicity of ANCA. Functional and observational analyses of ANCA subsets in blood samples from AAV patients gave contradictory answers to this question and are superficially taken as a hint that all human IgG subclasses are pathogenic. Existing *in vivo* models use polyclonal sera from MPO-immunized mice to induce an AAV-like phenotype in kidneys of naïve mice. Recently, Viehmann et al. developed the first *in vivo* model of AAV affecting the lung by applying anti-MPO monoclonal antibodies. This model permitted me for the first time to study subclass-specific pathogenicity of anti-MPO antibodies *in vivo*. In contrast to hyperimmune sera from immunized mice, monoclonal antibodies bind to very few distinct epitopes on the target antigen MPO. Considering the subclasses of mAbs used in the established model as well as preliminary observations in a model of anti-PR3 induced pulmonary vasculitis, I hypothesized that the pathogenicity of ANCA could depend on specific subclasses acting via FcγRIV in mice. Due to the distinct IgG subclass specificity of FcγRIV, murine IgG2, which specifically binds to FcγRIV and is the equivalent of human IgG1, was included into the study. To address subclass-specific effects of ANCA-like mAbs, IgG1 which does not bind to FcγRIV was chosen as the second subclass for this study.

To investigate the specific pathogenicity, benefits of the the single-chain format of antibodies (scFv-Fc) should be used. The design of constructs encoding for the C_H2 and C_H3 regions of IgG from different subclasses enables easy subclass changes of a variety of monoclonal antibodies. Given the knowledge about the sequence of the variable regions, the epitope-specific part of any antibody can be fused to the constant regions of different subclasses.

2. Material

2.1 Instruments and equipment

Autoclave	Varioklav, H+P Labortechnik, Oberschleissheim, Germany
Balances	PM 4800 Delta Range, Mettler-Toledo, Columbus, OH, USA
	2001 MP2, Sartorius, Göttingen, Deutschland
Centrifuges	5417R, Eppendorf, Hamburg, Germany
	5417C, Eppendorf, Hamburg, Germany
	Rotanta 460R, Hettich, Tuttlingen, Germany
	Rotanta/R, Hettich Tuttlingen, Germany
Gel electrophoresis	Bio-Rad, Hercules, California, USA
	Invitrogen, Carlsbad, California, USA
	Amersham-Pharmacia, Buckinghamshire, United Kingdom
Incubation shaker	HT Multitron, Infors, Bottmingen, Switzerland
Incubator	BBD6220, Heraeus, Thermo Scientific, Waltham, MA, USA
Icemachine	Ziegra, Isernhagen, Germany
Laminar flow	LaminAir HB 2472S, Heraeus, Hanau, Germany
Magnetic stirrer	MR3003, Heidolph, Kelheim, Germany
	KMO2 basic, IKA, Staufen, Germany
Microplate reader	FLUOStar Optima, BMG Labtech, Offenburg, Germany
	SunriseTM, TECAN, Maennedorf, Switzerland
Microscope	Leica DM IL, Leica Microsystems, Wetzlar, Germany
pH-meter	Inolab pH Level 1, WTW, Weilheim, Germany
PCR cycler	T3 Thermocycler, Biometra, Göttingen, Germany
Semidry blotter	Biometra, Göttingen, Germany
Shakers	130 basic, IKA, Staufen im Breisgau, Germany
	260 basic, IKA, Staufen im Breisgau, Germany

Spectrophotometer	ND-1000, peqlab, Erlangen, Germany
	Biophotometer, Eppendorf, Hamburg, Germany
Thermoblock	Thermomixer 5436, Eppendorf, Hamburg, Germany
Tissue processor	Microm STP 420D, Thermo Scientific, Waltham, MA, USA
Ultrasonic bath	Sonorex digital 10P, Bandelin, Berlin, Germany
Water bath incubator	MA6, Lauda, Lauda-Königshofen, Germany
Water preparation	Milli Q Advantage, Millipore, Billerica, MA, USA

2.2 Consumables

Consumables such as pipette tips, centrifuge tubes, reaction tubes, and microwell plates were procured from the following suppliers:

BD Biosciences (Franklin Lakes, NJ, USA)

Biozym (Hessisch Oldendorf, Germany)

Corning (Corning, NY, USA)

Eppendorf (Hamburg, Germany)

Mettler Toledo (Columbus, OH, USA)

Thermo Fisher Scientific (Waltham, MA, USA)

2.3 Chemicals

If not stated otherwise chemicals were purchased from the following suppliers:

BD Biosciences (Franklin Lakes, NJ, USA)

Bio-Rad Laboratories (Hercules, CA, USA)

Biozym (Hessisch Oldendorf, Germany)

Life Technologies (Carlsbad, CA, USA)

Merck (Darmstadt, Germany)

New England Biolabs (Ipswich, MA, USA)

GE Healthcare (Little Chalfont, Buckinghamshire, UK)

Qiagen (Hilden, Deutschland)

Roth (Karlsruhe, Germany)

Sigma-Aldrich (St Louis, MO, USA)

Thermo Fisher Scientific (Waltham, MA, USA)

2.4 Oligonucleotides

2.4.1 Gene blocks (gBlocks) designed for the study

Gene block	**Encoded region**
gBlock migg1	C_H2 and C_H3 region of IgG1 heavy chain
gBlock migg2a	C_H2 and C_H3 region of IgG2a heavy chain
gBlock scFv 4B12	V_H-$(GGGGS)_3$-V_L of mAb 4B12
gBlock scFv 5B11	V_H-$(GGGGS)_3$-V_L of mAb 5B11
gBlock V_H 4B12	V_H of mAb 4B12
gBlock V_H 5B11	V_H of mAb 5B11
gBlock κ-6D1	Full light chain of mAb 6D1
gBlock κ-6G4	Full light chain of mAb 6G4
gBlock IgG1 6D1	V_H of mAb 6D1, constant region IgG1 heavy chain
gBlock IgG2c 6D1	V_H of mAb 6G4, constant region IgG2c heavy chain
gBlock IgG1 6G4	V_H of mAb 6D1, constant region IgG1 heavy chain
gBlock IgG2c 6G4	V_H of mAb 6G4, constant region IgG2c heavy chain

2.4.2 Primers designed for the study

Method	Primer location	Sequence 5'-3'	Primer
Sequencing	V_L for	GAT ATT GTG MTC ACC CAR WCT MCA*	DJ3717
	V_L rev	CTC ATT CCT GTT GAA GCT CTT GAC	DJ3718
	V_H for	SAR GTN MAG CTG SAG SAG TCW GG*	DJ3719
	IgG1 C_H1 rev	ATA GAC AGA TGG GGG TGT CGT TTT GGC	DJ3727
	IgG2a C_H1 rev	CTT GAC CAG GCA TCC TAG AGT	DJ3716
	IgG2b 3' rev	TTT ACC CGG AGA CCG GGA GAT	DJ3768
	IgG2c 3' rev	TTT ACC CAG AGA CCG GGA GAT	DJ3776
Cloning	4B12 V_L for	GGC CAC GTG TTG ATG ACC CAG ACT CCA CTC TC	DJ3742
	5B11 V_L for	GGC GAT ATC GTG ATC ACC CAG TCT CCA GCA AT	DJ3743
	C_L rev	ATG ACC GGT CTA ACA CTC ATT CCT GTT GA	DJ3741
	5B11 5' for	TTA TAT GCA TTG GGT GAA ACA ATC A	DJ3744
	4B12 5' for	GCG GTA CCA GGG TCG ACC GGC GAG GTG CAG CTG CAG CAG TCA GGA	DJ3730
	IgG1 3' rev	CAA CAC ACG TGA CCT TAG GAG TCA GA	DJ3745
	IgG2c 3' rev	ATG ACC GGT TCA TTT ACC CAG AGA CCG GGA	DJ3776
	pTT5 5B11 for	AAA AAC GAG GAG GAT TTG ATA TTC ACC TGG CCC GA	DJ3777
	pTT5 5B11 rev	GTC ACC GAG GAG CCA GTT GTA CCT CCA CAC ACG GGC GCC AGT GG	DJ3778

* degenerate primer, M = A,C; R = A,G; W = A,T; S = C,G; N = A,C,G,T

2.5 Bacterial strain

Strain	Genotype	Provider
DH5α	F– Φ80lacZΔM15 Δ(lacZYA-argF) U169 recA1 endA1 hsdR17 (rK–, mK+) phoA supE44 λ– thi-1 gyrA96 relA1	Thermo Fisher Scientific

2.6 Cell line

Cell line	Provider
HEK293EBNA	NRC Biotechnology Research Institute

2.7 Recombinant proteins

Protein	Provider	Catalog #
Murine FcγRIV	R&D Systems	1974-CD-050
Murine TNF-α	Peprotech	315-01A
Murine MPO	AG Jenne	-
Human PR3S195A	Lisa Hinkofer, AG Jenne	-

2.8 Antibodies

Method	Target	Provider	Catalog #	Dilution	Conjugate
IHC	Ly-6G (rat)	BioLegend	127602	1:200	-
	CD31 (rabbit)	Cell signaling	77699	1:100	-
	Mac-2	Cedar Lane	CL8942B	1:400	Biotin
	2° anti-rat	Vector	BA4001	1:300	Biotin
	2° anti-rabbit	Vector	BA1000	1:750	Biotin
ELISA	Mouse IgG light chain	Jackson Immuno Research	115-035-174	1:5000	HRP
	Poly-His-tag	Core facility mAb, Helmholtz Zentrum	-	1:800	HRP
FC	CD3e	BioLegend	100229	1:50	BV650
	CD4	BD	564298	1:400	BUV737
	CD8a	BD	564920	1:800	BUV805
	CD11b	BD	563553	1:100	BUV395
	CD11c	eBioscience	25-0114-82	1:200	PE-Cy7
	CD19	BioLegend	115543	1:100	BV786
	CD44	BioLegend	103047	1:200	BV605
	CD45	BioLegend	103144	1:100	AF594
	CD103	BioLegend	121418	1:100	PB
	Ly6B2	Bio-Rad	MCA771A7	1:400	AF700
	Ly-6G	BioLegend	127643	1:400	BV711
	MHC-II	BioLegend	107606	1:500	FITC
	NK1.1	BioLegend	108720	1:100	AF647
	SiglecF	BD	740158	1:200	BV510
	TCRβ	eBioscience	47-5961-82	1:100	APC/eF780
	TCRγ	BD	553178	1:200	PE
	Ter119	BioLegend	116228	1:200	PerCPCy5.5

3. Methods

3.1 Molecular biology methods

3.1.1 RNA isolation from hybridoma cells

Total RNA from 10^6 hybridoma cells was extracted using phenol-chloroform extraction. After incubation in 1 mL TRIzol® (Life Technologies) for 5 min at RT, 200 µL chloroform was added to the suspension, vortexed and incubated for 15 min at RT. The solution was centrifuged (13000 × *g*, 10 min, 4°C), and 500 µL isopropanol were added to the aqueous phase. After incubation for 15 min at RT and centrifugation (13000 × *g*, 10 min, 4°C) the RNA pellet was washed with 1 ml 70% ethanol, air-dried and resolved in 20 µL RNase-free water.
Alternatively, Monarch® Total RNA Miniprep Kit from New England Biolabs was used to extract RNA from hybridoma cells according to the manufacturer's instructions and stored at -80°C until use.

3.1.2 Amplification and sequencing of IgG heavy and light chains

cDNA of the variable regions of κ-light and IgG1 and IgG2a/c heavy chains was amplified using OneStep RT-PCR Kit (Qiagen, Hilden, Germany) with the gene-specific primers listed in section 2.4.2 according to the protocol provided by the supplier. After Sanger sequencing by Eurofins Genomics (Ebersberg, Germany) the resulting DNA sequences were translated into the respective amino acid sequences. Since degenerated forward primers were used in order to ensure efficient amplification of IgG heavy and light chain mRNA transcripts of unknown sequence, the N-termini were corrected for the top-matched germline V hit.

3.1.3 Polymerase chain reaction

For amplification of specific regions from DNA as template, Phusion® Polymerase (New England Biolabs) was used according to the manufacturer's instructions.

3.1.4 Restriction digest

To create ligation compatible DNA ends in plasmid DNA and codon optimized gene blocks (gBlock from IDT listed in section 2.4.1) endonucleases that recognize and cut specific DNA sequences were purchased from New England Biolabs. 1-5 Units (U) of enzyme were used to digest 1 µg of DNA in the specific buffer recommended by the supplier at 37°C for 1 h. Digested DNA fragments were analyzed by agarose gel electrophoresis and extracted from the gel as described in section 3.1.5.

3.1.5 Agarose gel electrophoresis

Separation of DNA fragments according to their molecular weight was performed by electrophoresis using 1% agarose dissolved by heating in TAE buffer as gel. SYBR Safe (Life Technologies) was added to the buffer with a dilution of 1:10000 before polymerization to visualize DNA by UV light. DNA samples were supplemented with loading buffer, pipetted into the gel pockets and the gel was run at 60 V for 30-45 min. In order to determine the sizes of the DNA fragments a molecular weight standard (Gene Ruler 1kb, Fermentas, Thermo Scientific) was included for comparison.

3.1.6 DNA purification from agarose gels

DNA bands with the correct size were cut from the agarose gel and extracted by QIAQuick Gel Extraction Kit (Qiagen, Hilden, Germany) according to the manufacturer's instructions. 20 µL 52°C warm nuclease-free water was used to elute DNA from the columns to increase the concentration and yield of the purified DNA.

3.1.7 Determination of DNA/RNA concentration

After purification the concentration of DNA or RNA was determined by measuring the absorbance of 2 µL sample at 260 nm on a NanoDrop®. Purity of the sample was determined by measuring the optical absorbance at 280 and calculating the ratio of absorbance at 260/280.

3.1.8 DNA ligation

For the ligation of the digested insert DNA into 50 ng of digested vector with compatible DNA ends, T4 DNA Ligase (Thermo Scientific) was used for 1 h at RT or o.n. at 16°C in the recommended buffer with a reaction volume of 20 µL. The amount of insert for a vector to insert ratio of 1:5 was calculated with the following equation:

$$50\ \text{ng (vector)} \times 5 \times \frac{\text{length in bp (insert)}}{\text{length in bp (vector)}} = \text{m in ng (insert)}$$

3.1.9 Transformation of $CaCl_2$-competent *E. coli*

$CaCl_2$-competent *E. coli* of the DH5α strain were thawed on ice and 50 µL were mixed carefully with 4 µL of the ligation mix. After 30 min incubation on ice a heat-shock was performed for 50 s in a 42°C water bath and immediately chilled on ice for 10 min. 250 µL LB medium which was pre-warmed to 37°C were added to the *E. coli* and they were shaken at 37°C for 1 h. 200 µL were plated onto pre-warmed LB agar plates containing 100 µg/mL ampicillin as selection antibiotics and incubated over night at 37°C.

	Component	Concentration
LB medium (pH 7,5)	Yeast extract	5 g/L
	Tryptone	10 g/L
	Sodium chloride	10 g/L

3.1.10 Plasmid preparation from *E. coli* culture

For the multiplication and small-scale preparation of DNA plasmids single *E. coli* colonies that were transformed with the respective plasmids were grown overnight at 37°C in a shaking

incubator in 5 mL LB medium containing ampicillin. For large-scale preparations colonies were grown in 5 mL LB for 3 h at 37°C and the culture was transferred into 200 mL LB and incubated at 37°C overnight. QIAprep Spin Miniprep Kit (Qiagen, Hilden, Germany) or PureLink™ HiPure Plasmid Maxiprep Kit (Thermo Fisher Scientific, Waltham, Massachusetts) were used for DNA isolation according to the manufacturer's instructions. DNA was eluted from the spin columns with 52°C warm nuclease-free water to increase the yield of the purified DNA.

3.2 Protein expression and analysis

3.2.1 Protein expression in HEK293EBNA cells

For transient expression of recombinant proteins, HEK293 EBNA cells were transfected with polyethyleneimine (PEI) at a density of 10^6 cells per mL of culture. 1 µg of plasmid DNA and 2 µg PEI per mL of culture was incubated in Optipro serum-free medium (Thermo Fisher Scientific, Waltham, Massachusetts) for 20 min at RT before they were dropped slowly to the HEK293EBNA cells. For the production of two-chain mAbs the content of the cDNA transfected was modified as follows: heavy and light chain plasmids were co-transfected in equal amounts and supplemented by a five-fold amount of non-coding empty pTT5 plasmid to minimize the translation and folding load of recombinant antibody. The transfected cell culture was incubated with shaking at 37°C for 96 h. 24 h after transfection Bacto TC Lactalbumin Hydrolysate (BD Biosciences, Franklin Lakes, New Jersey) dissolved in H_2O was added to the cells to a final concentration of 0,5%. Supernatants containing the expressed protein were harvested by centrifugation and filtered through 0,2 µm filters.

3.2.2 Ni-NTA affinity chromatography

Supernatants containing recombinant protein were dialyzed overnight at 4°C against a 10-fold volume of binding buffer containing 20 mM Na_2HPO_4 and 300 mM NaCl (pH 7,4). HisTrap HP columns (GE Healthcare, Chicago, Illinois) equilibrated with binding buffer were used to purify

the recombinant proteins by interaction with the C-terminal His-tag. After washing the column bound protein was eluted with a gradient of 20 mM-1 M Imidazole in binding buffer, dialyzed against PBS and 0,2 µm sterile-filtered. Purity was assessed by SDS-PAGE stained with Coomassie Brilliant Blue or western blot and protein concentration was determined by BCA protein assay (Pierce, Thermo Fisher Scientific, Waltham, Massachusetts).

3.2.3 Protein deglycosylation by PNGase F

To analyze glycosylation of proteins, N-linked glycans were removed by Peptide:N-glycosidase F (PNGase F) (NEB, Ipswich, Massachusetts) in the buffer provided by the supplier. Three micrograms of protein were denatured for 5 min at 95°C, cooled on ice and subsequently incubated with PNGase F for 2 h at 37°C. The molecular weights of deglycosylated protein and the same amount of protein, not digested with PNGase F, were compared on an SDS gel as described in 3.2.4.

3.2.4 Sodium dodecyl sulfate-polyacrylamide gel electrophoresis

Analysis of proteins according to their molecular weight was performed by discontinuous SDS-PAGE using either self-casted gels or NuPAGE 4-12% Bis-Tris SDS gels (Invitrogen). Before protein samples were run on self-casted gels in Tris-glycine running buffer or purchased gels in MOPS running buffer they were supplemented by either reducing or non-reducing sample buffer. Samples where reducing sample buffer was used were denatured for 5 min at 95°C before being loaded on the gel. Molecular weight determination of the analyzed proteins was performed by comparison to PeqGold prestained protein marker V (PEQLAB Biotechnologie GmbH).

Buffer	Component	Concentration
Tris-glycine running buffer (pH 8,6)	Tris (free base)	50 mM
	glycine	384 mM
	SDS	0,2%

MOPS running buffer (pH 8,2)	MOPS (free acid)	30 mM
	Tris (free base)	60 mM
	SDS	0,2%
	Sodium Bisulfite	6,5 mM
4x reducing sample buffer	Tris (free base)	200 mM
	SDS	10%
	Glycerol	40%
	ß-Mercaptoethanol	30%
	Bromophenol blue	0,2%
4x non-reducing sample buffer	Tris (free base)	200 mM
	SDS	10%
	Glycerol	40%
	Bromophenol blue	0,02%

3.2.5 Coomassie staining

For the visualization of proteins on SDS gels, Coomassie Brilliant Blue was used. After 1 h incubation in Coomassie solution followed by 30-60 min incubation in destaining solution the gel was imaged in a ChemiDoc imaging system (Biorad, Hercules, California).

Solution	**Component**	**Concentration**
Coomassie staining solution	Coomassie Brilliant Blue	0,25%
	Methanol	45%
	Acetic acid	10%
Destaining solution	Methanol	45%
	Acetic acid	10%

3.2.6 Silver nitrate staining

For more sensitive detection of proteins in SDS gels, the proteins were fixed in the gel for 1 h. The gel was washed three times for 20 min in 50% ethanol, incubated with 0,2 g/L $Na_2S_2O_3x5H_2O$ for 1 min and rinsed with tap water three times. After incubation with silver nitrate solution in the dark for 20 min and three more washes with tap water proteins were visualized by developing solution. The reaction was stopped when the intensity of protein bands was sufficient and the gel was subsequently imaged in a ChemiDoc system.

Solution	Component	Concentration
Fixation solution	Methanol	50%
	Acetic acid	12%
	Formaldehyde	0,0185%
Silver staining solution	Silver nitrate	0,2 g/L
	Formaldehyde	0,028%
Developing solution	Sodium carbonate	60 g/L
	Sodium sulfate	4 mg/L
	Formaldehyde	0,002%
Stop solution	Methanol	50%
	Acetic acid	12%

3.3 Immunological methods

3.3.1 Enzyme-linked immunosorbent assay (ELISA)

Direct ELISA was used to analyze IgG affinities to specific proteins. Nunc Maxi Sorb Plates were coated at 4°C o.n. with the protein of interest (5 µg/mL) followed by blocking with 3% BSA and 4 h incubation at RT with increasing concentrations of IgG. Bound antibody was detected with peroxidase-conjugated κ-light chain-specific secondary antibody. TMB was used as substrate and binding affinity was analyzed spectrophotometrically at OD 450 nm corrected

by OD 540 nm. For the detection of anti-MPO IgG, recombinant mMPO was coated and a standard curve of anti-MPO IgG with known concentration was included for quantification.

3.3.2 Western blotting

Proteins separated by SDS-PAGE were transferred to a PVDF membrane by semi-dry western blotting in order to detect individual proteins by binding of specific antibodies. After activating the membrane in methanol for 30 s it was assembled with the SDS gel between two Whatman filter papers soaked in transfer buffer and placed onto the cathode plate of the blotting chamber. The transfer from the gel onto the membrane was carried out at constant current of 400 mA for 50 min. Unspecific binding was blocked by 5% milk powder (Sigma Aldrich, St. Louis, Missouri) in PBS for 1 h at RT. Since western blots were performed only for the analysis of recombinant mAbs, no primary antibody was used. The membrane was therefore directly incubated with HRP-coupled goat-anti-mouse secondary antibody and proteins were detected subsequently by Merck™ Luminata™ Crescendo Western HRP-Substrate and imaged on a ChemiDoc imaging system.

3.3.3 Flow cytometry

Flow cytometry was performed in collaboration with S. Viehmann (Institute of Experimental Immunology, University Clinic of Bonn, Rheinische Friedrich Wilhelm University, Bonn, Germany).

Cells were incubated with fluorochrome-conjugated antibodies (listed in section 2.8) in FACS-blocking buffer (3% FCS, 0,1% NaN_3, 5% human poly Ig) for 20 min on ice. After three times washing with PBS the cells were analyzed with a BDCanto II (Becton Dickinson) and absolute cell numbers were determined using FlowJo 10 software. In order to be able to quantify cell numbers, 5 x 10^3 counting beads (CaliBRITE™ BD Biosciences, Franklin Lakes, NJ, USA) were added to each cell suspension before FACS analysis. Dead cells were excluded by Hoechst staining.

3.4 *In vitro* neutrophil oxidative burst assay

To test the ability of anti-MPO IgGs to trigger ROS production in neutrophils, PMNs were isolated from C57BL/6 mice and resuspended at a concentration of 4 x 10^6 cells/mL. Neutrophils were primed for 15 min at 37°C with 10 ng/mL TNF-α (Peprotech, Rocky Hill, New Jersey) before anti-MPO IgGs were added at concentrations of 40-80 µg/mL. In addition, 150 µM Dihydrorhodamine 123 (DHR) were added to the neutrophils as ROS indicator. DHR can passively diffuse through membranes and can be oxidized by ROS to rhodamine 123 which exhibits fluorescence at 488 nm.

After incubation for 1 h at 37°C, the cells were stained with neutrophil-specific fluorochrome-conjugated Ly6G-antibody and analyzed by flow cytometry.

3.5 Mouse model analysis

Injections, sample collection (BALF, plasma and lung tissue), measurement of hemoglobin and flow cytometry were performed by S. Viehmann (Institute of Experimental Immunology, University Clinic of Bonn, Rheinische Friedrich Wilhelm University, Bonn, Germany).

3.5.1 Isolation of PMNs from mouse bone marrow

After sacrificing one C57BL/6 mouse by cervical dislocation, the femurs were dissected, the bones were cut at both ends and the bone marrow (BM) was flushed out with 5 mL RPMI medium (Gibco®, Thermo Fisher Scientific, Waltham, Massachusetts) using a 26G x ½" needle. The pooled BM was centrifuged (500 *x g*, 5 min), washed with RPMI and the BM suspension was sent through a cell strainer to disperse the cells. 5.69 mL HBSS and 9.32 mL Percoll (GE Healthcare) were used to underlie the suspension before centrifugation (500 *× g*, 30 min,4 °C, no break). Erythrocytes were subsequently lysed in lysis buffer for 3 min at RT and the cells pelleted by centrifugation (500 *x g*, 5 min). After washing with RPMI, the isolated PMNs were counted with a hemocytometer.

	Component	Volume
Red blood cell lysis buffer	0,16 M NH_4Cl	9 mL
	0,17 M Tris-HCl pH 7,5	1 mL

3.5.2 Study approval

C57BL/6 mice were purchased from The Jackson Laboratory and maintained under SPF conditions at the animal facilities of the University Hospital Bonn. 8-12 weeks old female mice were used for *in vivo* experiments. All animal experiments were approved by governmental committees (Landesamt für Natur, Umwelt und Verbraucherschutz, NRW).

3.5.3 Induction of pulmonary vasculitis *in vivo*

Mild inflammation was triggered in the lungs of 10 weeks old female C57BL/6 mice by intratracheal injection of 10 µg fMLP and 10 µg LPS in 50 µL PBS. Simultaneously the first dose of anti-MPO antibodies containing 50 µg 6D1 and 50 µg 6G4 in 200 µL PBS was injected intraperitoneally. One group of 5 mice received both antibodies in the IgG1 subclass, another group of 5 mice both antibodies in the IgG2c subclass. As control, two groups of 5 mice each received equivalent amounts of IgG1 or IgG2c isotype control antibodies. The antibody injection was repeated on 3 consecutive days two times per day resulting in a total amount of 600 µg IgG per mouse. On day 5 after the first injection mice were sacrificed by Xylazine (20 mg/kg) and Ketamine (200 mg/kg) in 200 µl PBS and samples were collected.

3.5.4 Sample collection

Bronchoalveolar lavage (BAL) was performed by instilling three times 1 mL 2 mM EDTA in PBS into the trachea. After hemoglobin quantification in the BAL fluid (BALF), BAL supernatant and BAL cells were obtained by centrifugation (450 *x g*, 15 min, 4°C). The lung was perfused

with 1 mL 10% neutral buffered formalin, collected and incubated overnight at 4°C. The fixed lung tissue was shipped in 70% ethanol at RT. At the time of sacrifice blood was taken from the heart and plasma was collected using heparin as anticoagulant. Measurement of hemoglobin levels as well as flow cytometry was performed immediately after sample collection. Plasma and BAL supernatant were shipped on dry ice and stored at -80°C until analysis.

3.5.5 Quantification of pulmonary hemorrhages

Hemoglobin levels in 75 µl BALF were measured spectrophotometrically at 400 nm with background subtraction at 670 nm.

3.5.6 Preparation of lung tissue for histological analysis

The left lobe of fixed mouse lungs was dissected and cut horizontally into 4 pieces which were processed in an automated tissue processor resulting in specimens being fully infiltrated with liquid paraffin. Subsequently the tissue was embedded in paraffin, cooled on a cooling plate and stored at RT until use.

3.6 Histology and Immunohistochemistry

For histopathological and immunohistochemical analyses, sample blocks formalin-instillation-fixed, paraffin-embedded lung tissue were submitted to the Core Facility Tissue Analytics and Pathology of the Helmholtz Zentrum München. Histopathological examinations were performed on tissue sections of 3 µm nominal thickness, stained with hematoxylin and eosin (H&E, standard stain). Special stains were applied for differentiation of different types of infiltrating leucocytes (giemsa-stain), as well as for detection of interstitial collagenous connective tissue (Masson's trichrome stain) (Romeis, 2015). All histological stainings were performed according to established standard protocols, using a HistoCore SPECTRA ST slide

stainer (Leica, Germany) with prefabricated staining kits. Immunohistochemical detections of CD31 (a marker of vascular endothelial cells), LyG6 (a marker of neutrophils), and MAC2 (a marker of macrophages) were performed (Noll and Schaub-Kuhnen, 2000) on a Ventana Discovery Ultra-stainer (Roche Diagnostics, Germany), using specific antibodies and prefabricated reagents (Ventana Kit DAB-MAP, Roche, Germany). All immunohistochemical analyses included appropriate positive and negative controls. The applied antibodies and dilutions are specified in section 2.8.

4. Results

4.1 Generation of recombinant monoclonal anti-hPR3 antibodies

Preliminary observations made from the model of anti-hPR3 induced pulmonary vasculitis in transgenic hPR3-humanized mice, gave rise to the suggestion that the specific subclass of PR3-specific mAbs injected in mice determined their pathogenicity *in vivo* (Hinkofer et al., unpublished data). Based on two anti-hPR3-specific mAbs used in these preliminary experiments, recombinant anti-hPR3 mAbs in different subclasses were initially considered for further explorations at the beginning of my project.

All gene blocks (gBlocks) and primers used for the generation of recombinant monoclonal anti-hPR3 antibodies are listed in section 2.4.1 and 2.4.2, respectively.

4.1.1 Sequencing of anti-hPR3 antibodies from hybridoma cells

In order to create different subclasses for the same anti-hPR3 mAbs, the sequence of the specific variable regions of the antibodies experimentally used by our collaborators to induce pulmonary vasculitis in mice, had to be determined. The two mAbs 4B12 and 5B11 from hybridoma cell lines that were produced by the core facility of monoclomal antibodies (Helmholtz Zentrum München) were determined to belong to the IgG2a and IgG1 subclass, respectively. On base of the conserved constant region within each subclass as well as in the light chains, the reverse primers for the amplification of the critical variable domains were chosen inside the C_H1 and C_L regions. Degenerate forward primers were designed that allowed for a high number of mismatches when binding to the highly variable framework regions. These degenerate primers contain equimolar mixtures of two or more different bases at a given position within the primer sequence and can thus prime the unknown 5'-sequence which codes for the N-terminal amino acid residues of the heavy and light chains. The variable regions of 4B12 and 5B11 were successfully amplified from mRNA of the respective hybridoma cell lines

and the sequences, where the degenerate primer hybridized were corrected in accordance with the top V germline hit (Figure 3).

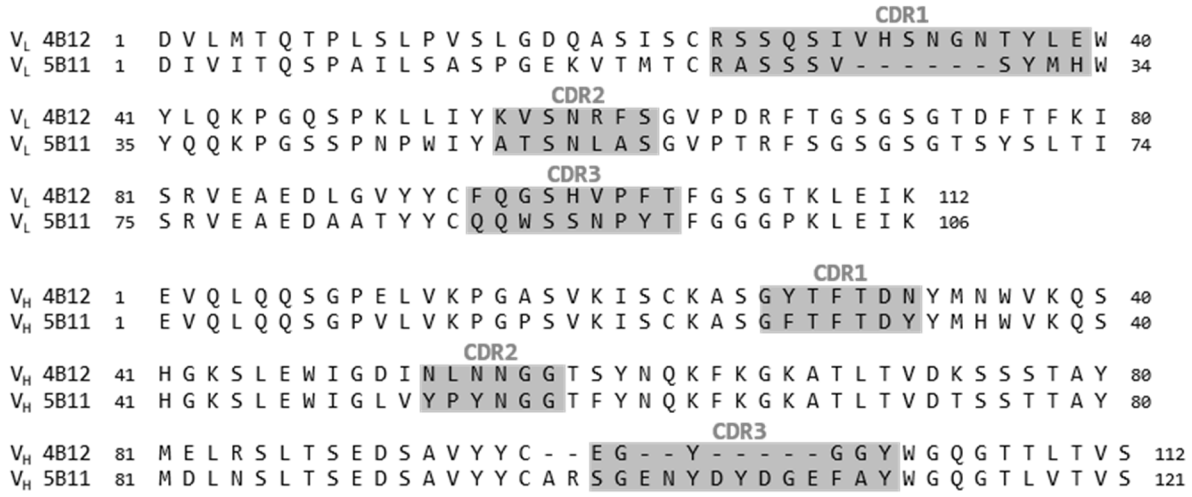

Figure 3: Amino acid sequences of anti-hPR3 antibodies. Alignment of variable light chain (V_L) and variable heavy chain (V_H) amino acid sequences of the sequenced anti-hPR3 antibodies 4B12 and 5B11. CDRs are highlighted in grey.

4.1.2 Production of single-chain scFv-Fc anti-hPR3 antibodies

For the production of the single-chain scFv-Fc antibodies of IgG1 and IgG2a subclasses, gene blocks (gBlocks) encoding C_H2 and C_H3 of murine IgG1 and IgG2a were cloned into the pTT5 expression vector. Using the sequences of the variable regions of light and heavy chains (Figure 3), specific gene blocks for 4B12 and 5B11 were designed that encode for V_H and V_L regions connected by a flexible peptide linker. The obtained V_H-$(GGGGS)_3$-V_L cDNA was cloned into the constructs for the constant regions of IgG1 and IgG2a resulting in sets of vectors for the production of epitope-matched scFv-Fc mAbs 4B12 and 5B11. The used pTT5 vector encodes for an Igκ-signal peptide at the N-terminus of the scFv-Fc mAbs which leads to secretion of correctly folded protein into the supernatant of transfected HEK293EBNA cells. Several attempts to express the single-chain antibodies in these cells resulted in poor yields of mAb in the supernatant (Figure 4A, left western blot panel).

To obtain enough mAb for binding studies to the target antigen hPR3, the supernatant was concentrated. Even a 1000-fold amount of scFv-Fc antibody did not bind efficiently to hPR3 in comparison to the native mAb from hybridoma supernatant as determined by direct ELISA (Figure 4B, red bar).

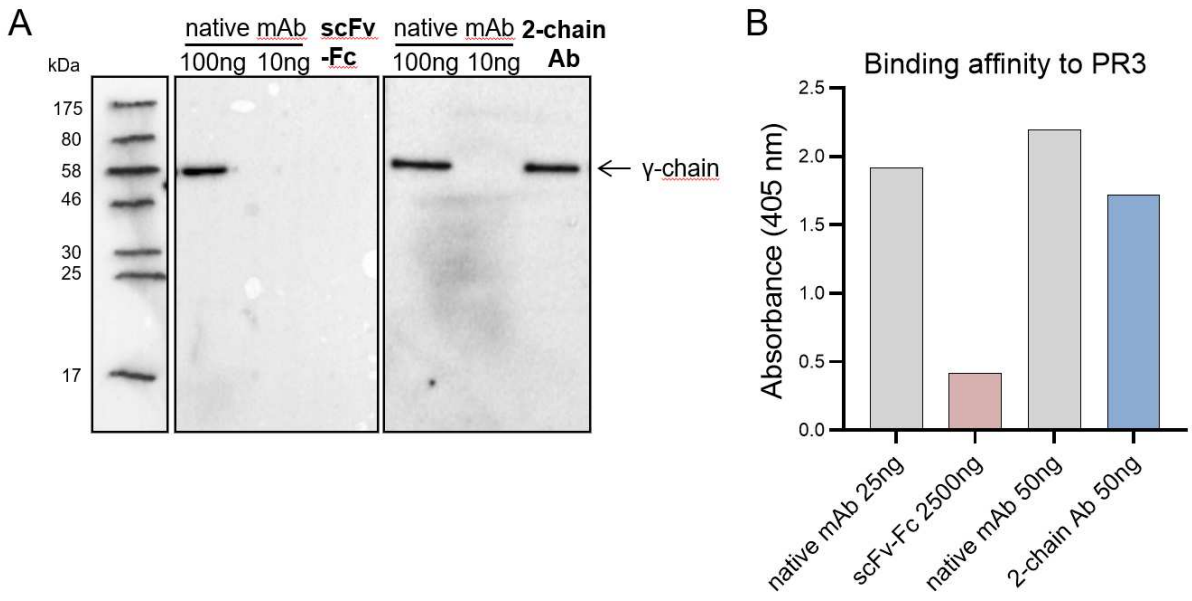

Figure 4: Expression and binding properties of recombinant single-chain and two-chain mAbs against hPR3. (A) Western blot analysis of the expression of scFv-Fc and 2-chain anti-hPR3 mAb. 20 µL supernatant of cells expressing the respective antibody were compared to 100 ng and 10 ng of native hybridoma antibody. **(B)** Binding of scFv-Fc and 2-chain mAbs to recombinant hPR3 was compared to the native hybridoma mAb by direct ELISA with the coated target antigen hPR3.

4.1.3 Production of two-chain anti-hPR3 antibodies

Since the production of the recombinant single-chain format of anti-hPR3 antibodies was not successful, I decided to switch to the naturally occurring IgG structure consisting of full heavy and light chains (in the following called two-chain mAb). For this purpose, full heavy and light chains needed to be cloned into separate vectors. Primers located at the 5' and 3' end of the sequence encoding for the respective antibody chains were designed, full lengths chains were

amplified from hybridoma mRNA and cloned into pTT5. For the subclass switch of 5B11 from IgG1 to IgG2a, and 4B12 vice versa, gBlocks were designed and cloned into pTT5 vector. When the clones were sequenced to verify the correct insert DNA, I found some parts of the heavy chain sequence of IgG2a to differ from published sequences for the constant region of this subclass. More intensive analysis revealed the hybridoma antibody 4B12 to be of IgG2c subclass instead of IgG2a. Consultation of the core facility of antibodies (Helmholtz Zentrum München), that generated the anti-hPR3 clones, confirmed this finding. The hybridoma cell lines were generated from C57BL/6 mice, which do not have the allele for IgG2a antibodies. Thus, the clone 4B12 was erroneously determined as IgG2a.

Since the gBlock used for the production of the IgG2a heavy chain was based on the sequence of IgG2a, this construct needed to be converted to the sequence of IgG2c. Amplification of the variable region specific for 5B11 from the existing vector and subcloning into the vector containing IgG2c 4B12 resulted in the correct cDNA for IgG2c 5B11.

Co-transfection of equal amounts of heavy and light chains of the individual antibodies in HEK293EBNA cells resulted in poor yields of two-chain mAb in the supernatant and massive aggregation inside the transfected cells (data not shown). To minimize the amount of translated mAb in the cells and thereby decrease the folding load, the empty pTT5 vector without any insert was included in the co-transfection. A ratio of mAb encoding pTT5 and empty pTT5 of 1:10 was determined to be the most efficient transfection mix for high yields of mAb. Using a C-terminal His-tag attached to light chains, recombinant mAb preparations were purified from the supernatant of transfected cells 96 h after transfection. Semi-quantitative analysis by western blot estimated the presence of 100 ng recombinant mAb in 20 µL of cell culture supernatant (Figure 4A, right western blot panel). This results in a yield of 5 µg/mL of transfected cell culture. Direct ELISA showed that the binding of two-chain anti-hPR3 antibody towards the target antigen is equal to the native mAb from hybridoma cells (Figure 4B, blue bar).

4.1.4 Anti-hPR3 4B12 binds with high affinity to poly-His-tag

For the *in vivo* application of recombinant anti-hPR3 mAbs and the investigation of anti-PR3 induced pathogenic effects, cross-reactions of the anti-hPR3 antibodies with MPO, the essential target antigen in MPA-AAV had to be excluded. Therefore, binding studies of 5B11 and 4B12 towards recombinant human and murine PR3 and MPO were performed by direct ELISA. MAb 4B12 bound efficiently to all tested antigens. A common feature of all recombinant antigens used for immunization of mice and binding studies was a Hexa-His-tag which had been attached to the C-terminus to facilitate purification of the recombinant proteins. Further analysis in the group of U. Specks, revealed that 4B12 indeed primarily binds to the poly-His-tag (Pang et al., unpublished data). Using untagged hPR3, however, moderate binding of 4B12 could also be detected. A theoretical model based on computational simulations confirmed the observed binding specificity (Pang et al., unpublished data).

4.2 Recombinant production of monoclonal anti-MPO antibodies

Apart from our collaborative efforts to establish an *in vivo* model for anti-PR3-associated vasculitis, Viehmann et al. also aimed at establishing a robust experimental model for anti-MPO-induced pulmonary vasculitis. Due to the limitation of reproducibility of the hPR3-induced model for AAV as well as the unwanted His-tag specificity of our anti-hPR3 monoclonal antibody, I decided to shift my focus to investigations on murine MPO-specific antibody subclasses. Due to the experiences I gained from the recombinant production of anti-hPR3 scFv-Fc mAbs, which showed poor expression and target binding, only the two-chain format of anti-MPO mAbs was included in the subsequent course of my project. The two monoclonal antibodies, 6D1 and 6G4, purified from hybridoma supernatants, were capable of inducing pulmonary vasculitis in mice as shown by our collaborator meanwhile. In view of these positive results with anti-MPO mAbs, I started to produce these two mAbs as recombinant two-chain IgG1 and IgG2c antibodies.

4.2.1 Sequencing and production of anti-MPO mAbs

Hybridoma cells secreting the mAbs 6D1 and 6G4 of the IgG2b and IgG2c subclass, respectively, were kindly provided by Peter Heeringa (University Medical Center Groningen, The Netherlands). To ensure that the subclasses of the two mAbs have been determined correctly, new reverse primers which hybridize to the 3' end of the DNA sequences, encoding the heavy and light chains, were designed and used for sequencing. The degenerate forward primers designed and already used by myself for the cloning of anti-hPR3 antibodies were fully suited to amplify and sequence the cDNA of the anti-MPO mAbs.

The 5'-sequences of the heavy and light chains sequences, were derived from germline V sequences best matching our partial cDNAs. GBlocks were designed for the light chains as well as for two sets of heavy chains and cloned into pTT5 vector for the production of four recombinant mAbs, 6D1 and 6G4, in the IgG1 and IgG2c subclass formats. The amino acid sequences of V_L, V_H for the two clones 6D1 and 6G4 as well as C_H regions of IgG1 and IgG2c heavy chains are shown in Figure 5.

Like with the anti-hPR3 two-chain mAbs, the highest yields of anti-MPO mAbs in the supernatant of HEK293EBNA cells were obtained by co-transfecting empty vector at a ratio of 1:10. After 96 hours of expression anti-MPO IgGs were purified from the supernatant by Ni-NTA affinity chromatography with the help of the His-tag attached to the C-terminus of the light chains.

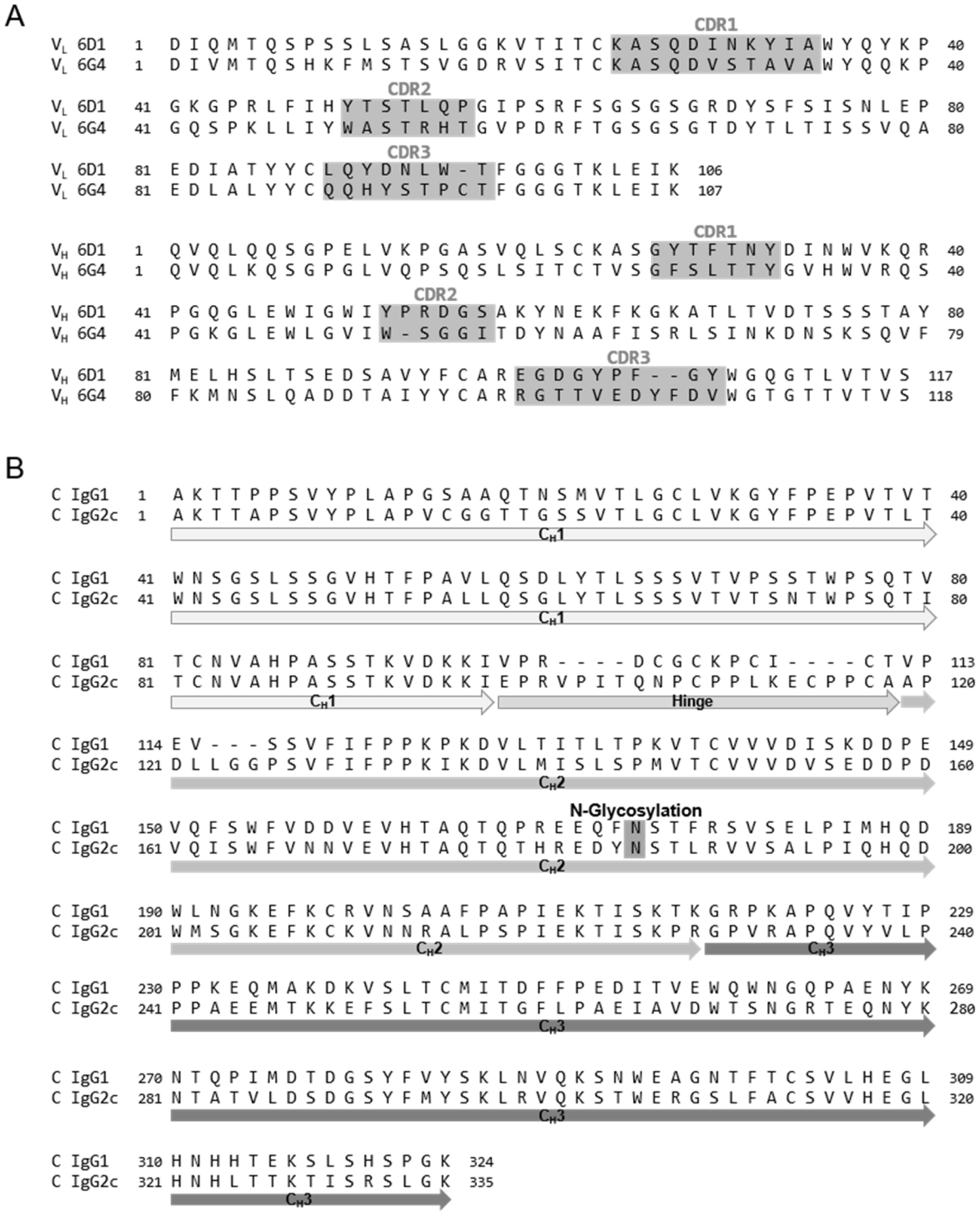

Figure 5: Amino acid sequences of anti-MPO antibodies. (A) Alignment of variable light chain (V_L) and variable heavy chain (V_H) amino acid sequences of 6D1 and 6G4, CDRs are highlighted in grey. **(B)** Alignment of heavy chain amino acid sequences of IgG1 and IgG2c subclasses. Arrows below the amino acid sequences mark the individual C_H regions (C_H1, C_H2, C_H3); the glycosylated residue (N) is highlighted by a grey background.

4.2.2 Characterization of recombinant anti-MPO mAbs

Purified recombinant IgG as well as native hybridoma mAb were deglycosylated by PNGase F, an enzyme which removes all N-linked carbohydrates, and were analyzed by SDS-PAGE. In parallel, equal amounts of each antibody were run on the same SDS-Gel under reducing and non-reducing conditions (Figure 6A). Overall, the pattern of recombinant mAb preparations was comparable to that of the native mAbs. No free heavy and light chains could be detected under non-reducing conditions (NR), which indicated to us that all purified antibody forms were correctly assembled as IgG tetramers. The band intensities of heavy and light chains under reducing conditions (R) agreed with those of the native mAb which indicated the same stoichiometry of heavy and light chains in the recombinant IgG tetramers. After deglycosylation (DG) a shift in the mass of heavy chains was noticed, whereas this shift was not seen for the light chains. These findings were consistent with the light and heavy chain sequences. Only one N-glycosylation site was present in the IgG heavy chains which is known to be highly conserved. Removal of the attached glycan by PNGase F leads to a decrease of molecular mass, discernible by the downward shift of heavy chains in all preparations. These observations are fully consistent with the conclusion that the recombinant anti-MPO mAbs were indeed glycosylated, which is essential for proper binding to FcγRs. To characterize the anti-MPO mAbs further, binding studies were performed by ELISA. The binding properties of both native antibodies, 6D1 and 6G4, to the target antigen mouse MPO showed no significant difference (Figure 6B, left graph). Comparisons of recombinant IgG2c antibody preparations with the respective native IgG2b and IgG2c antibodies showed no significant difference in their binding capacity at different dilutions. IgG1 mAbs, however, displayed slightly reduced binding to MPO when compared with the native mAb. This was observed for both mAbs, 6D1 and 6G4 (Figure 6B, middle and right panel). Comparison of the binding of recombinant IgG1 and IgG2c anti-MPO did not show any significant difference for both epitope-matched sets of mAbs. Potential effects of the mAbs of individual subclasses, thus, do not depend on a differential binding to the target antigen MPO. This finding establishes an important base for this study, in

which the potential of recombinant anti-MPO mAbs of different subclasses to induce a vasculitis-like phenotype in mice should be investigated.

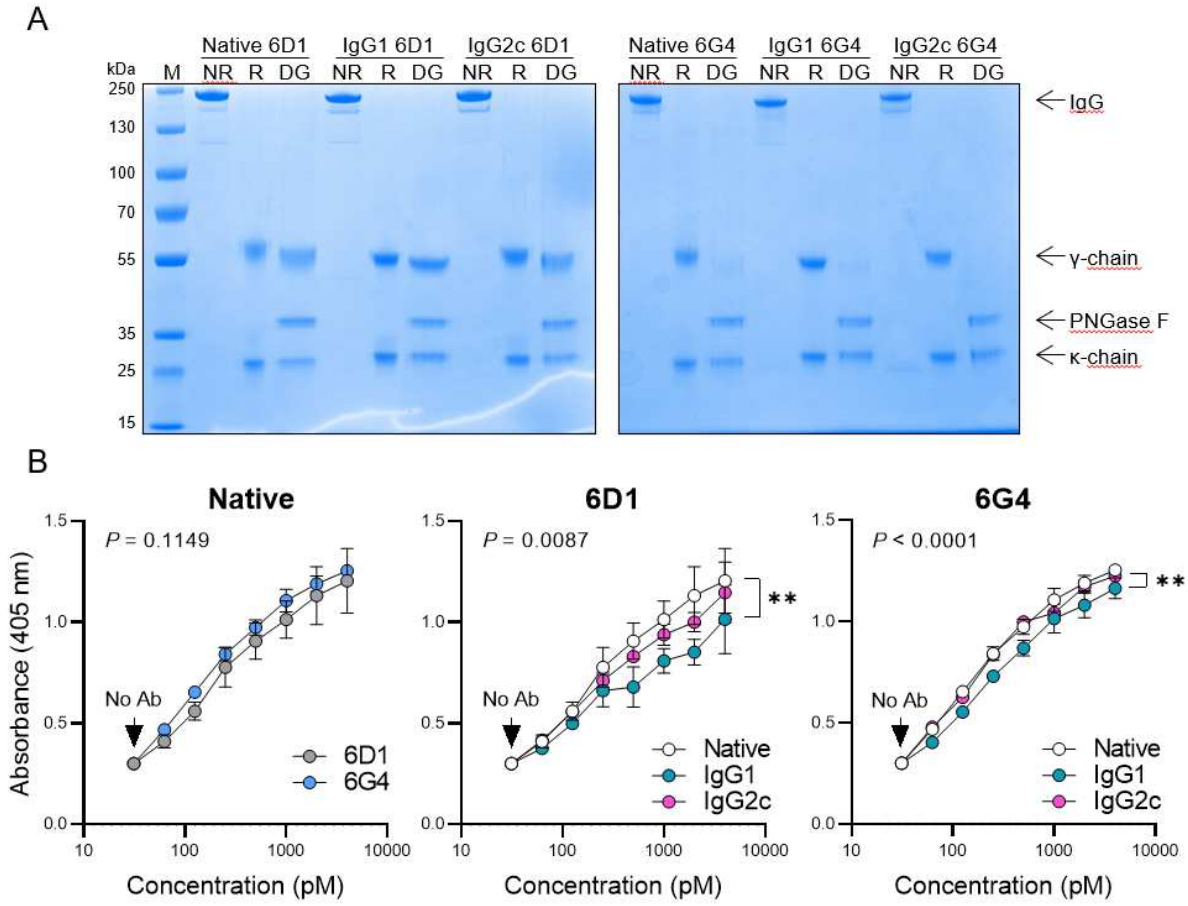

Figure 6: Characterization of recombinant anti-MPO IgG1 and IgG2c antibodies. (A) Coomassie-stained SDS-PAGE of native and recombinant IgG1 and IgG2c mAbs 6D1 and 6G4 under non-reducing (NR) and reducing (R) conditions and after deglycosylation (DG) with Peptide-N-Glycosidase F (PNGase F). **(B)** Concentration-dependent binding of native and recombinant IgG1 and IgG2c antibodies to mMPO measured by direct ELISA. Values represent the mean ± SEM absorbance at 405 nm of 3 technical replicates; *P*, overall probability by two-way ANOVA. Significant differences between native and recombinant IgG1 mAbs are shown. ** $P < 0.01$ by Turkey's multiple comparison test.

To characterize not only the affinity of the recombinant mAbs to the target antigen but also the potential to interact with FcγRIV, a binding study was performed by ELISA. Recombinant mAbs targeting the same epitope but differing in their subclasses showed differential binding towards

FcγRIV. While the native anti-MPO clone 6G4 (originally IgG2c) as well as the recombinantly produced IgG2c anti-MPO mAb showed high and comparable binding to the FcγRIV receptor, binding of the recombinant IgG1 mAb of the same clone could not be observed (Figure 7).

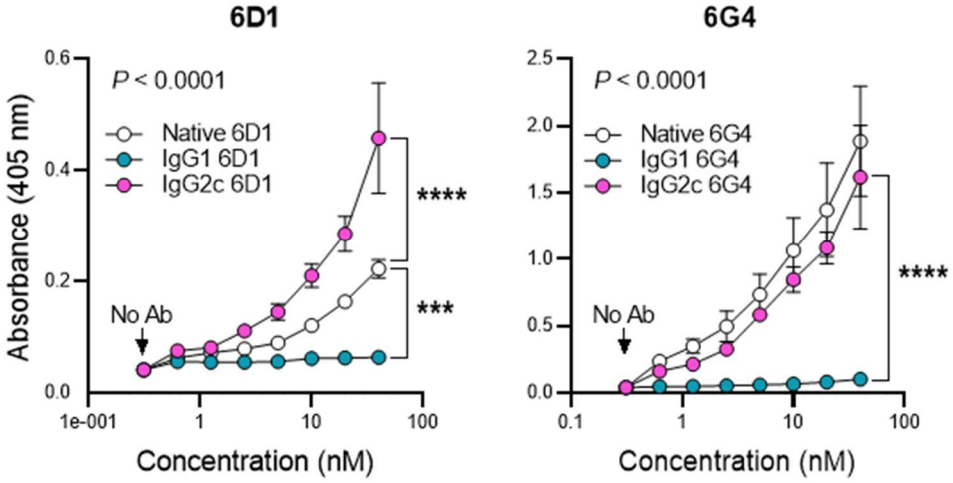

Figure 7: Binding of recombinant IgG1 and IgG2c anti-MPO as well as native mAb to FcγRIV. Data are shown as mean ± SEM of technical duplicates and compared by by two-way ANOVA, ***, and **** represent $P < 0.001$ and $P < 0.0001$ for the indicated comparisons by Turkey's multiple comparison test.

4.3 Subclass-specific effects of anti-MPO mAbs

4.3.1 Monoclonal antibodies to MPO do not induce neutrophil oxidative burst *in vitro*

The pathogenicity of ANCA is broadly believed to depend on their capacity to induce oxidative burst in neutrophils. To test this pathogenic effect of different anti-MPO antibodies of the subclasses IgG1 and IgG2c *in vitro*, an assay based on the dye dihydrorhodamine 123 (DHR) was performed (Figure 8A). DHR has a lipophilic property, which allows it to easily enter subcellular compartments of a cell. ROS are able to oxidize DHR to the fluorescent compound rhodamine 123 which can be detected by fluorescence readers or flow cytometry.

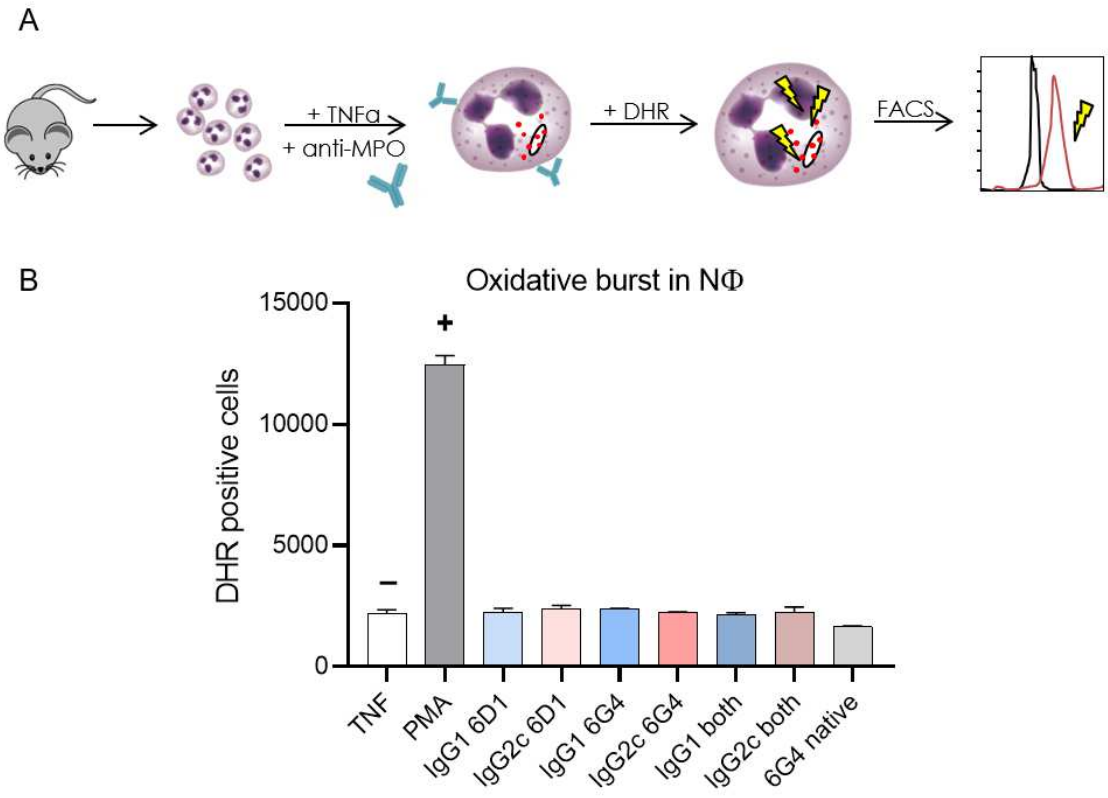

Figure 8: Monoclonal antibodies are not able to induce oxidative burst in mouse neutrophils. **(A)** Schematic of the *in vitro* assay for neutrophil oxidative burst. BM neutrophils of C57BL/6 mice were primed with TNF-α and incubated with mAbs or PMA as positive control. DHR was used to detect ROS production and the number of ROS producing neutrophils was determined by flow cytometry. **(B)** No significant difference in DHR positive cells can be detected after incubation with different anti-MPO mAbs. Ordinary one-way ANOVA and Turkey's multiple comparison test were used for statistical analysis of technical duplicates. – represents the negative control, + represents the positive control with PMA.

To initiate the translocation of MPO to the surface of neutrophils, isolated from the bone marrow of C57BL/6 mice, the purified cells were primed with murine TNF-α before incubation with the mAbs of different subclasses. To imitate conditions of the established *in vivo* model, which uses a combination of two different mAbs, 6D1 and 6G4, this combination two different mAbs were also tested. As controls the native antibody 6G4 as well as phorbol myristate acetate (PMA), which strongly induces an oxidative burst in neutrophils, were included. The number of DHR positive cells significantly increased when neutrophils were incubated with the

stimulator PMA, compared to neutrophils that were only primed with TNF-α (Figure 8B). For all tested mAbs and mAb combinations, however, no effect could be observed.

4.3.2 Application of recombinant anti-MPO mAbs *in vivo*

To test the subclass-specific pathogenicity of anti-MPO antibodies *in vivo* the recombinant mAbs were applied systemically to C57BL/6 mice (experiments performed by S.F. Viehmann, University of Bonn). Based on the established model of pulmonary vasculitis, the same combination of mAbs against MPO, 6D1 and 6G4, was used. It is known that infectious triggers like *S. aureus* infections, initiate inflammatory responses and thereby can reduce immune tolerance and favor the development of AAV (Scully et al., 2012). For this reason, low dose lipopolysaccharide (LPS) and N-formyl-L-methionyl-L-leucyl-L-phenylalanine (fMLP) were injected intratracheally into the lungs of mice to mobilize and attract neutrophils. Simultaneously, a first dose of recombinant anti-MPO mAbs was injected into the peritoneum. One group of five mice received both recombinant mAbs expressed as a two-chain murine IgG1 antibody, while a second group of five mice was treated with the same pair of mAbs of the murine IgG2c subclass. Two control groups (five mice in each group) treated with equivalent amounts of IgG1 (C_{IgG1}) or IgG2c (C_{IgG2c}) isotype control antibodies were included, to exclude a general antibody-dependent effect. Isotype control antibodies are directed against bacterial proteins, which should not be present in the mice, as they are kept under specific-pathogen-free (SPF) conditions. In order to maintain a disease-relevant steady level of "ANCA", the model of Viehmann et al., which applies a high 1 mg dose of total anti-MPO IgG, was adapted. On three consecutive days, 100 µg consisting of a 1:1 mixture of 6D1 and 6G4 mAb or a control mAb, was injected twice per day, resulting in a cumulative dose of 600 µg antibody per mouse. On day 5 after the first injection mice were sacrificed, samples were collected and analyzed for parameters of a vasculitic phenotype (Figure 9A).

4.3.2.1 Administration of anti-MPO mAbs of different subclasses causes distinct reactions in mice.

In order to exclude highly variable steady state levels which could account for the observed phenotype difference in the two comparison groups, anti-MPO IgG levels were measured in the plasma of all differentially treated mice. No significant difference in the mAb concentrations was observed between the two treatment groups of mice receiving either IgG1 or IgG2c anti-MPO antibodies (Figure 9B). Furthermore, the presence of endogenous anti-MPO IgG in the blood circulation has been excluded by these measurements, since no anti-MPO IgGs were detected in the plasma of mice treated with isotype control mAbs.

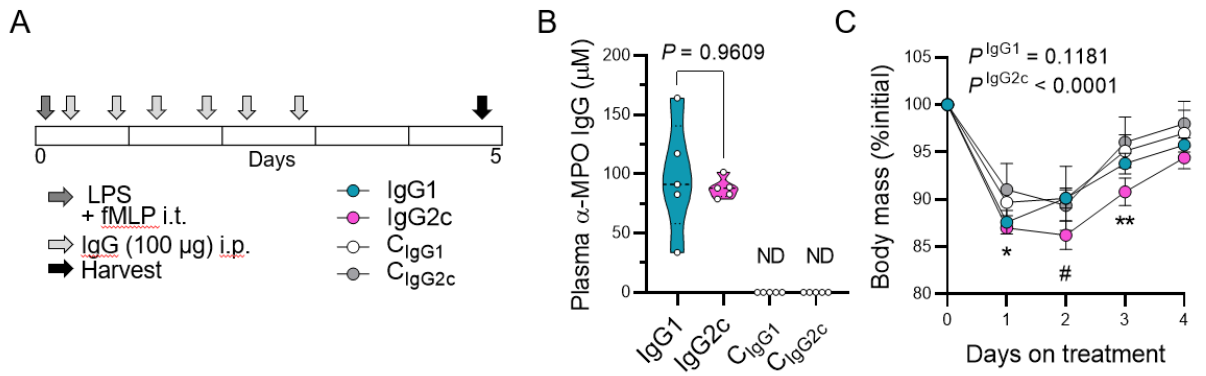

Figure 9: Injection of anti-MPO mAbs produces similar plasma levels of anti-MPO IgG but the body mass differs between the two treatment groups. n=5 per group **(A)** Experimental setup of LPS and fMLP injections which initiate a mild lung inflammation followed by six IgG injections on 3 consecutive days. **(B)** Plasma anti-MPO concentrations determined by direct ELISA. *P*, probability determined by one-way ANOVA. **(C)** Mean ± SEM for the body mass compared with the values on day 0 before treatment in percent. P^{IgG1}, probability between IgG1 and C_{IgG1}; P^{IgG2c}, probability between IgG2c and C_{IgG2c}, as determined by ordinary one-way ANOVA. * $P < 0.05$ and ** $P < 0.01$ for the comparison of IgG2c to C_{IgG2c} and # $P < 0.05$ for the comparison of IgG2c to all other groups by Turkey's multiple comparison test.

As a result of lung inflammation induced by the local application of LPS and fMLP, a reduction of the body weight was observed in all animals already 1 day after injection. While mice of the

IgG1 group regained weight already on the following day, weight loss in the group receiving IgG2c anti-MPO persisted and a significant reduction in bodyweight on day 2 compared to IgG1-treated mice was observed (Figure 9C #). Furthermore, the overall recovery of IgG2c-treated mice was slower compared to IgG1 and control groups. This effect can be specifically attributed to anti-MPO antibodies of the IgG2c subclass, since mice receiving IgG2c isotype control mAb significantly regained weight in contrast to anti-MPO specific IgG2c-injected mice (Figure 9C *).

4.3.2.2 IgG2c anti-MPO causes pulmonary hemorrhages in mice

The main readout for experimental induced pulmonary vasculitis is the occurrence of pulmonary hemorrhages. Mice that received IgG2c anti-MPO showed a significantly higher amount of blood in the lungs compared to IgG1- and isotype control-treated animals, as determined by the spectrometric analysis of the hemoglobin content in the bronchoalveolar lavage (BAL) (Figure 10A). This finding was confirmed by the total count of red blood cells (RBC) in the BAL (Figure 10B).

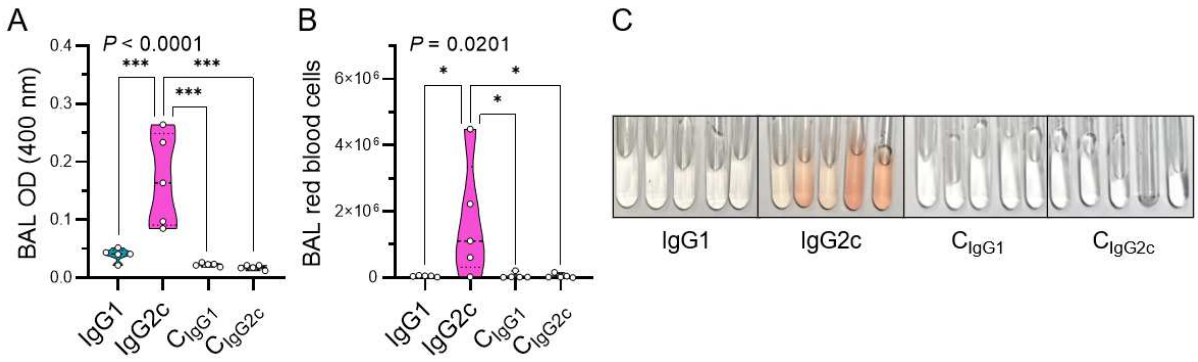

Figure 10: IgG2c anti-MPO causes pulmonary hemorrhages in mice. (A) Hemoglobin levels of BAL measured by absorbance at 400 nm (demonstrated by images of BAL in **C**). **(B)** Total red blood cell counts in BAL. *P*, overall probability by ordinary one-way ANOVA. * $P < 0.05$ and *** $P < 0.001$ for the indicated comparisons by Turkey's multiple comparison test.

4.3.2.3 IgG2c anti-MPO leads to immune cell infiltration and inflammation in the lung

Beside pulmonary hemorrhages, pulmonary vasculitis is associated with immune cell infiltration into the lung tissue. To analyze this typical inflammatory phenotype, BAL cells of the mice treated with IgG1 and IgG2c anti-MPO mAbs as wells as isotype control antibodies were analyzed by flow cytometry. Normalized to the numbers of total leucocytes (CD45 positive cells) neutrophils are enriched in the BAL of mice from the IgG2c-treated group (Figure 11A). An even higher enrichment can be seen for eosinophils, which are a hallmark of EGPA (Figure 11B). Inflammation is always associated with increased expression of proteins like cytokines and their presence in the affected tissues and organs. Furthermore, the concentration of protein in the BAL fluid is a marker for vascular permeability and cellular damage within the lung. Protein levels in the BAL of anti-MPO treated mice is significantly increased when IgG2c-treated mice are compared to the group receiving the respective IgG1 subclasses (Figure 11C). This increase in protein levels can be specifically attributed to the alterations in the lungs, as the amounts observed in the BAL were normalized to the levels of total plasma protein.

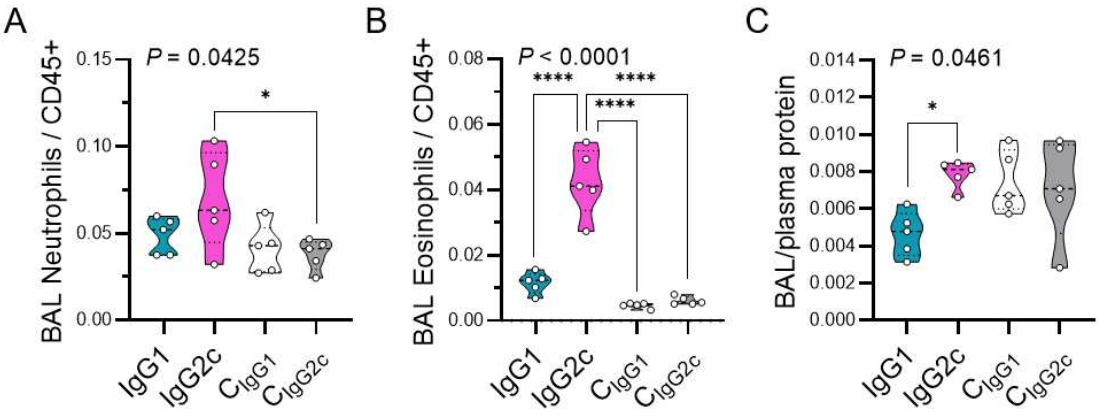

Figure 11: IgG2c anti-MPO causes immune cell infiltration and inflammation in mouse lungs. Ratio of BAL neutrophils **(A)** and eosinophils **(B)** to total leukocytes. **(C)** Ratio of BAL to plasma total protein. *P*, overall probability by ordinary one-way ANOVA. * $P < 0.05$ and **** $P < 0.0001$ for the indicated comparisons by Turkey's multiple comparison test.

4.3.2.4 IgG2c anti-MPO causes a vasculitis-like phenotype in lung tissue

Histopathological analysis of lung tissue was performed by H&E staining of lung tissue from all treated animals. Mild histological alterations were present in all experimental groups but can be graded as artefacts due to the intratracheal instillation of fixation solution.

The histopathological alterations present in the examined sections of mice treated with IgG1 or IgG2c anti-MPO as well as isotype control mAbs, in general displayed a moderate variation between different mice of the same experimental groups. The overall phenotype, however, was distinct for each group.

Since alterations in lung pathology were predominantly exhibited by sections of IgG2c anti-MPO-treated animals, representative images of only this group are presented in Figure 12.

In pulmonary sections of mice receiving isotype controls only mild to focally moderate expansion of alveolar septae and the presence of few numbers of mixed inflammatory cells could be observed. Besides macrophages, lymphocytes, and granulocytes few plasma cells were present within the alveolar septae and the alveolar spaces (Figure 12A,C,D). Furthermore, moderate numbers of extravascular erythrocytes could be observed in the alveolar spaces.

Animals treated with IgG2c anti-MPO showed variable hyperemia and inflammatory alterations, occasionally centered on small vessels. Some of these vessels demonstrated hypertrophic endothelial cells, which indicates activation of the endothelium (Figure 12D). Of note is that inflammatory foci seem to be often centered around remnants of degenerate vessels (Figure 12*). Furthermore, patchy and occasionally marked alveolar hemorrhage, as well as noticeable and diffuse thickening of alveolar septae was present in this group. This thickening can be attributed to edema, extracellular matrix (ECM) deposition, scant fibrin and the presence of extra- and intravascular pulmonary macrophages as well as few granulocytes (Figure 12D). In addition, expansion of the alveolar spaces due to hemorrhage, edema fluid, and infiltrating alveolar macrophages could be observed.

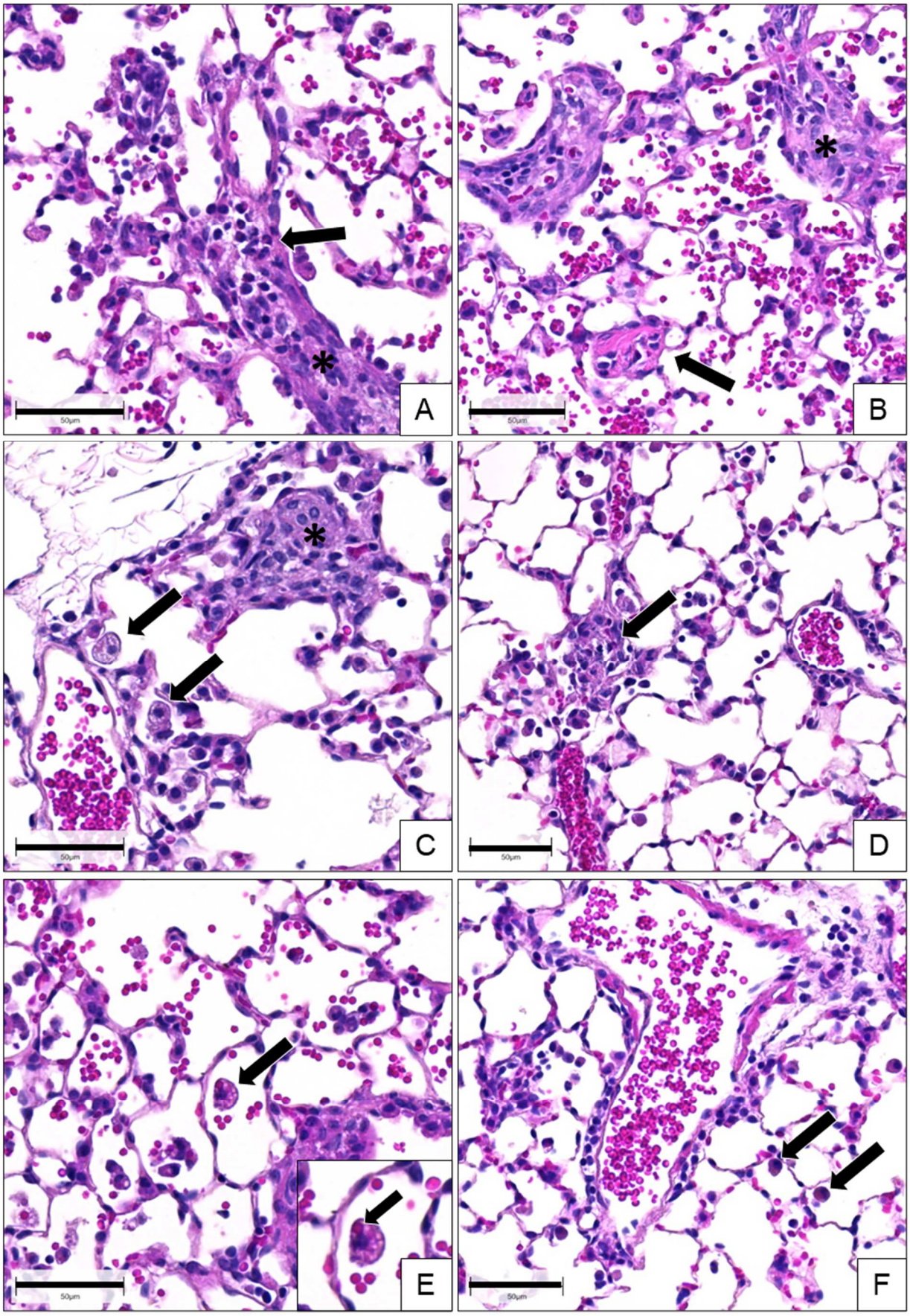
A
B
C
D
E
F

Figure 12: Histopathological observations on lung sections from IgG2c MPO-treated mice.
(A) Intact granulocyte infiltrating the vascular wall of an inflamed small pulmonary vessel. **(B)** Arrow marks fibrinoid necrosis (presumably) of a small vessel wall. **(C)** macrophages are present in the lumen of alveoli. **(D)** inflammatory focus with fibrin exudation, hemorrhage and infiltration of macrophages and granulocytes. **(E)** Intra-alveolar erythrocytes and macrophages, some of which phagocytosed erythrocytes. **(F)** Arrows mark the hemosiderin-loaded macrophages. FFPE tissue, HE stained. **(*)** asterisks mark inflammatory foci centered around degenerate small vessels. Scale bars represent 50 µm. © Core facility of tissue analytics and pathology 2019.

Interestingly, some of these macrophages contained phagocytosed erythrocytes (Figure 12E, insert) and hemosiderin which results from the degradation of hemoglobin (Figure 12F). Moreover, hyperplasia of type II pneumocytes which give rise to type I pneumocytes after epithelial damage in the alveoli was present in some sections (Figure 12E). Few perivascular and peribronchiolar lymphocytic infiltrates were present in the lung tissue and occasionally also follicular infiltrates of lymphoplasmacytic nodules could be observed.

Some of the above described phenomena were also seen in lung tissue of IgG1 anti-MPO-treated mice. Their extent and abundance, however, was markedly increased in the IgG2c anti-MPO-treated group, which displayed noticeably exacerbated lesions as compared to the IgG1-treated group.

4.3.2.5 Staining of specific cell types confirms inflammatory pulmonary vasculitis caused by IgG2c anti-MPO treatment

In order to analyze the observed histological alterations in more detail, specific immunostainings were performed. An overview of H&E-stained sections of lung tissue is shown in Figure 13 and shows strong inflammation and infiltration of cells into the lung tissue in IgG2c-treated mice while in the other groups this effect is largely absent. Vascular damage of small vessels, presumably capillaries, was detected by specific staining of endothelial cells. CD31-positive cells can be observed in in the center of inflammatory foci, showing the remnants of alveolar capillaries in the affected tissue.

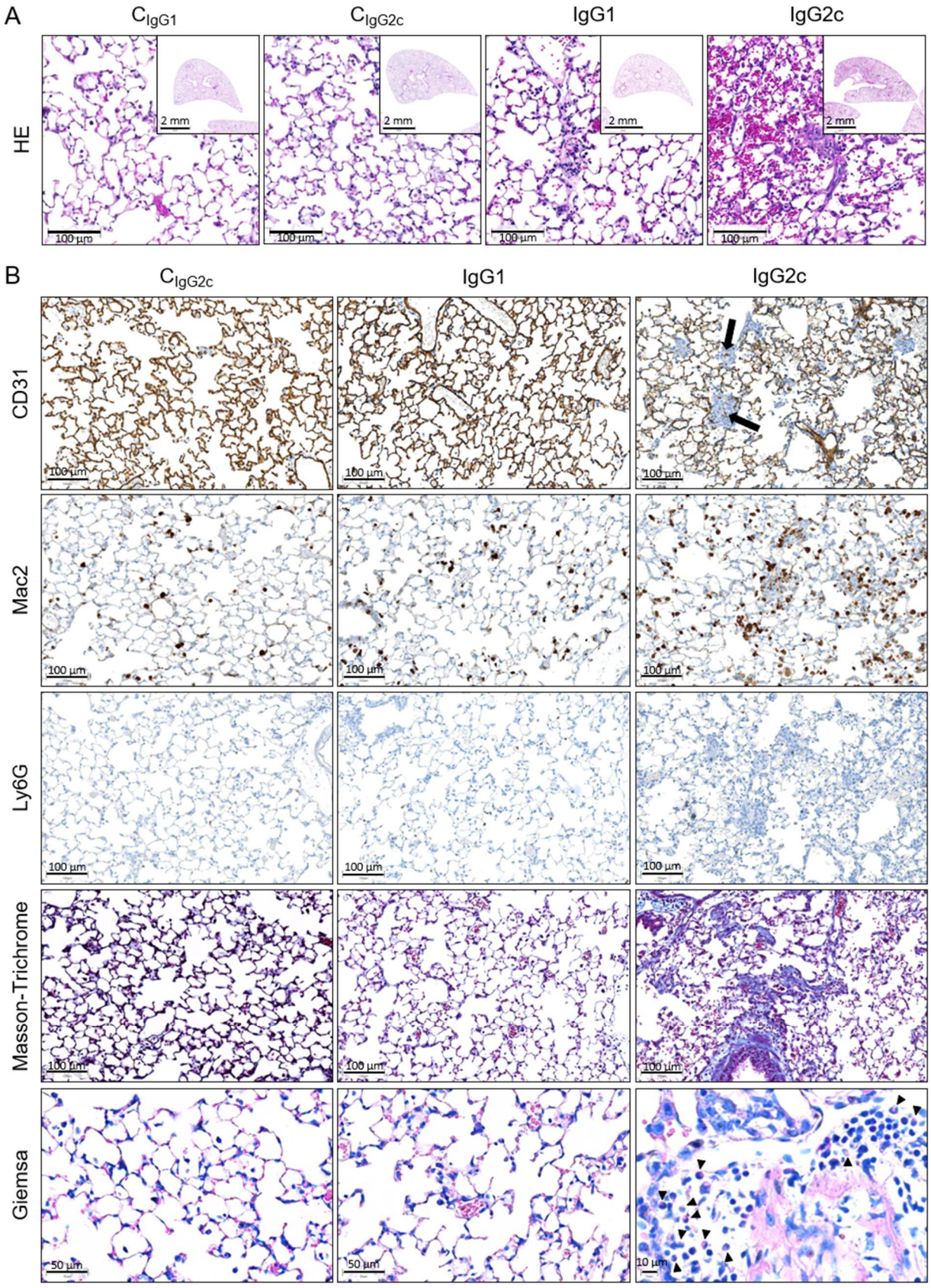
A
C IgG1
C IgG2c
IgG1
IgG2c
HE
2 mm
100 µm
B
C IgG2c
IgG1
IgG2c
CD31
Mac2
Ly6G
Masson-Trichrome
Giemsa
100 µm
50 µm
10 µm

Figure 13: Immunohistochemical analysis of lung tissue from anti-MPO and isotype control-treated mice. (A) Overview of HE-stained sections of lung tissue shows strong inflammation and infiltration of cells into the lung tissue in IgG2c-treated mice while in the other groups this effect is largely absent. **(B)** Specific immunostainings display the presence and abundance of endothelial cells (CD31+), with small vessel damage especially in the foci of inflammation (indicated by arrows). While Infiltrating macrophages (Mac2) are quite abundant neutrophils (Ly6G) are mainly absent in the lung tissues. Masson-trichrome staining shows the deposition of the ECM protein collagen and Giemsa staining demonstrates the differential abundance of granulocytes within the affected tissue. Arrow heads indicate eosinophilic granulocytes, especially abundant in the IgG2c group. © Core facility of tissue analytics and pathology 2020.

As already observed in the aforementioned H&E analysis, the predominantly present immune cell type, not only within the inflammatory lesions, were macrophages, as determined by Mac-2 staining. Their abundance in lung tissue within the IgG2c anti-MPO-treated group was markedly increased, as compared to the IgG1 and other control groups. On the other hand, Ly6G-stained neutrophils were largely absent in sections of all groups. Deposition of collagenous ECM in foci of inflammation in the lung tissue of IgG2c anti-MPO-treated mice could be vizualized by Masson-trichrome staining. Furthermore, the number of eosinophilic granulocytes subjectively exceeded the quantity of granulocytes, as determined by Giemsa staining. Since the pathogenic phenotype of both control groups were comparable, only representative images of C_{IgG2c} are shown in Figure 13.

5. Discussion

5.1 Generation of single-chain and two-chain monoclonal anti-hPR3 antibodies

5.1.1 Single-chain anti-hPR3 antibodies are not suitable for this study

The use of single-chain antibodies of the scFv-Fc format has attracted increasing attention for experimental studies about antibody-mediated mechanisms and specific effects of antibodies *in vivo* (Bujak et al., 2014, Nelson, 2010). The main advantage of single-chain antibodies utilized in these studies was the easy exchange of the epitope-determining variable regions in different subclass-specific frameworks to obtain an epitope-matched mAb of another subclass. Two mAbs directed against hPR3 have been previously produced by the hybridoma technology in the core facility of the Helmholtz Center Munich to study the effects of antibodies in a transgenic humanized model of hPR3 knock-in mice. Although both mAbs were directed against the same target antigen, they were found to induce differential effects in the lungs of mice sensitized with intratracheally applied low dose LPS (Hinkofer et al., unpublished data). The feature distinguishing the two mAbs was simply the subclass which they belong to.

To this end, a pair of two anti-hPR3 mAbs, named 4B12 and 5B11, has been produced as IgG1 and IgG2c antibodies for the continuation of this initial study. After several attempts to achieve sufficient quantities of single-chain antibodies the final amounts of scFv-Fc anti-hPR3 antibodies purified from HEK293EBNA supernatants were too small to perform *in vitro* and *in vivo* studies with mice (Figure 4A). In addition, the binding between these recombinant scFv-Fc antibodies and the target antigen hPR3 was found to be extremely low (Figure 4B). The single-chain formats of the anti-hPR3 clones 4B12 and 5B11, and moreover, single-chain formats in general, were therefore not considered appropriate for further investigations.

5.1.2 Two-chain anti-hPR3 antibodies were successfully produced

Since the use of single-chain antibodies was regarded as totally unrealistic for further investigations, the naturally occurring IgG structure consisting of two heavy and two light chains was instead prioritized for the continuation of the project. Relatively late, I also discovered that the anti-hPR3 clone 4B12 was falsely reported to us to be IgG2a subclass instead of the correct subclass IgG2c. The initial IgG2a constructs were subsequently modified to the IgG2c format and eventually both two-chain antibodies, 4B12 and 5B11, were successfully produced as a full length IgG1 and IgG2c antibody in HEK293EBNA cells (Figure 4A). By contrast to the respective single-chain Fv-Fc formats (V_H-V_L-C_H2-C_H3) for the same antibodies, the recombinant two-chain antibodies bound with high capacity to the target antigen hPR3 and this binding was comparable to that of the native clones (Figure 4B).

5.1.3 Anti-hPR3 antibody clone 4B12 does not specifically target hPR3

Further characterization of the recombinant mAbs towards hPR3 revealed that the clone 4B12 also showed high binding to other recombinant poly-His tagged fusion proteins. Even though this antibody also displayed a significant, but low reactivity with the untagged hPR3, it was not considered as a suitable candidate for the investigation of ANCA pathogenicity *in vivo*. This previously unrecognized cross-reactive binding behavior of an anti-hPR3 mAb may also lend support to the hypothesis that a promiscuous set of antibodies is triggered during the course of microbial infections, few of which then cross-react with similar epitopes on hPR3 from neutrophils (Pang et al., unpublished data).

5.1.4 Limitations

Anti-hPR3 antibody mAb 4B12 was shown to induce a GPA-like phenotype in the lungs of mice when it was injected intraperitoneally after low dose LPS instillation into the trachea of mice. In order to explore the impact and influence of PR3-specific antibody subclasses on their pathogenicity in mice, recombinant formats of the murine mAb 4B12 of the IgG2c subclass

and another hPR3-specific antibody, 5B11 of the IgG1 subclass – which was not pathogenic – were produced. Characterizing these mAbs in more detail, we discovered that mAb 4B12 did not primarily bind to hPR3, rather its major reactivity with the recombinant antigen was caused by its specificity to the attached poly-His tags. We, therefore, came to the conclusion that our key mAb 4B12, which this study should be based on, was not suited for the proposed investigations as we had envisioned initially.

The most decisive factor for this decision, however, was the fact that the first observations with the anti-hPR3 antibody 4B12 could not be reproduced. Other groups had also failed to establish an *in vivo* vasculitis model for GPA using monoclonal anti-hPR3 antibodies (Pfister et al., 2004; Schreiber et al., 2016). This could be due to the small amounts and poor accessibility of PR3 in mouse neutrophils and on their cellular surface even after priming. In contrast to humans, mouse neutrophils do not express PR3 on the surface under resting conditions (Korkmaz et al., 2008) and the general expression of PR3 in mice is relatively low. It was furthermore shown, that neutrophil activation is facilitated by the interaction of the neutrophil-specific receptor CD177 with PR3 on the membranes of resting human neutrophils (Jerke et al., 2011). This effect cannot be observed in mice since mouse PR3 is missing the homologous CD177 interacting site. In order to establish a functional GPA model *in vivo* Schreiber et al. (2016) generated a double-transgenic mouse line that expressed human PR3 as well as human CD177 on the surface of neutrophils under a heterologous human MRP-8 (S100A8) promoter. Attempts to induce a GPA-like phenotype in these mice by application of human anti-PR3 ANCA IgG as well as murine anti-hPR3 mAbs were, however, not successful (Schreiber et al., 2016). Interestingly, the mAbs used in this study were of the murine IgG1 and IgG2a subclasses. A subclass-specific effect, however, was not discerned since, overall, each mAb was individually tested and did not induce any pathogenic phenotype.

Altogether, the multiple challenges so far prevented researchers from establishing an anti-PR3 related *in vivo* model for the investigations of GPA.

5.2 Generation of two sets of epitope-matched anti-MPO antibodies

5.2.1 Production of functional anti-MPO IgG1 and IgG2c subclass antibodies

A robust model of pulmonary vasculitis induced by two anti-MPO mAbs simultaneously given, has been successfully established by Viehmann et al. (unpublished data). On base of this newly available tool the focus of studying subclass-specific effects of ANCA in AAV was switched to the investigation of anti-MPO antibodies. The two anti-MPO clones 6D1 (IgG2b) and 6G4 (IgG2c) induced a vasculitis-like phenotype in the lungs of mice, when they were applied in combination. Single application of the individual antibodies, however, did not induce a pathogenic phenotype. Monoclonal antibodies interact with only one epitope on the target antigen and form a binary complex. Effector signaling through interaction of the IgG Fc part with FcγRs, however, depends on receptor cross-linking through multiple closely spaced IgG molecules (Ortitz et al., 2016). In the anti-MPO induced pulmonary vasculitis model, the necessary proximity and density of FcγRs on the surface of effector cells was therefore achieved by a combination of two mAbs with different epitope specificities (Huugen, 2007).

Since both mAbs used belonged to the murine IgG2 subclass, it was decided to stick to the subclasses chosen previously for the anti-hPR3 antibodies.

Anti-MPO 6D1 and 6G4 have been sequenced and were successfully produced as recombinant IgG1 and IgG2c two-chain antibodies (Figure 5). Glycosylation of the IgG-Fc domain at the conserved N297 was previously shown to have an effect on the quaternary structure of the constant region. The resulting more open conformation was shown to be critical for the interaction with FcγRs (Sondermann et al., 2000). In the context of AAV it was shown that the glycosylation of ANCA indeed plays a critical role for their pathogenicity. Deglycosylation of anti-MPO ANCA by endoglycosidase S (EndoS) inhibited the induction of neutrophil degranulation *in vitro* and systemic application of EndoS attenuated the development of necrotizing and crescentic glomerulonephritis (NCGN) and vasculitis *in vivo* (van Timmeren et al., 2010).

Thus, the presence of critical glycosylations was analyzed for the recombinantly produced antibodies and compared to the native hybridoma clones. The essential glycan attached to the asparagine at position 297 of the IgG heavy chains increases their molecular mass by the weight of the sugar moieties. The total weight of the glycosylation contributes to 2-3% of the molecular weight of IgG (Arnold et al., 2007). After deglycosylation with PNGase F a shift in the mass of the heavy chain in all mAb preparations indicated that glycosylations were present after recombinant production in HEK293EBNA cells (Figure 6A). Weaker intensities of the bands after deglycosylation result from the additional steps performed, where the initially equal amount of mAb was decreased during several transfers between different vials.

The IgG molecule consisting of two heavy and two light chains is formed by a variable number of disulfide bonds, depending on the subclass, that connect the two heavy chains at the hinge region. Another disulfide bond between the C_H1 region of the heavy chains and the C_L region of the light chains links the heavy and light chains (Liu and May, 2010). Under non-reducing conditions, these connective bonds are intact and the IgG molecule has a molecular mass of around 150 kDa. Denaturation leads to the disassembly into heavy chains, with a mass of around 50 kDa, and the 25 kDa light chains. By comparison of the recombinant and native mAbs under reducing and non-reducing conditions on an SDS gel we came to the conclusion that fully assembled IgG tetramers were indeed present in all recombinant preparations, since no bands for free heavy and light chains could be detected.

Subclass-switch variants of a mAb towards glucuronoxylomannan have been previously analyzed. The authors noticed that the constant region of different subclasses has an impact on the conformation of the epitope-specific variable regions, and on the binding affinity to the target antigen (Torres et al., 2007). This effect was previously attributed to the highly flexible hinge region, which differs between IgG subclasses. In humans the subclass with the highest flexibility between antigen binding Fab arms is IgG3 > IgG1 > IgG4 > IgG2 (Roux et al., 1997). This flexibility mainly depends on the length of the hinge region. The hierarchy in flexibility of the murine IgG subclasses IgG2b > IgG2a > IgG3 > IgG1 is likewise determined by the length

of the hinge regions (Dangl et al., 1988). Murine IgG1 has the shortest hinge which comprises of only 12 amino acids, while the longest and most flexible hinge is found in IgG2b with 22 amino acids (Burton, 1985). This difference in the hinge region may account for the slightly better binding of the IgG2c mAbs 6D1 and 6D4 to MPO as compared to their epitope-matched IgG1 counterparts (Figure 6B, middle and right panel). This reduced binding of IgG1 mAbs was also observed when it was compared to the binding of the native mAbs of IgG2b and IgG2c subclasses, while no significant differences in the binding between the natural IgG2b/IgG2c and the recombinant IgG2c antibodies to a distinct epitope were detected.

Although recombinant IgG1 anti-MPO mAbs bound significantly weaker to MPO than the native epitope-specific mAbs, only a minor difference in binding between recombinantly produced mAbs of IgG1 and IgG2c subclasses was detected, however, this was statistically not significant. This enabled us to compare the recombinant mAbs based on their subclass-specific effects.

From the observed binding properties of the recombinant mAbs we can conclude that major differences in the pathogenicity of the recombinant anti-MPO mAbs can be attributed to the effector function via FcγR signaling rather than differential binding to the target antigen MPO.

Choosing these two specific subclasses of monoclonal antibodies we aimed to explore the impact of differential transcellular signaling through FcγRIV on myeloid effector cells *in vivo*. Furthermore, IgG2 consisting of IgG2a, IgG2b and IgG2c is the predominant murine subclass involved in pro-inflammatory processes, while in humans, antibodies of the homologous IgG1 as well as of the IgG3 subclass contribute most to inflammation (Reviewed in Nimmerjahn, 2006). Until now, the association constant of IgG2c to FcγRIV has not been determined. As shown in Figure 7, recombinant IgG2c anti-MPO showed strong binding to FcγRIV, while binding of the IgG1 subclass antibody could not be observed. This observation is in line with previous reports that likewise did not detect binding of IgG1 but reported high affinity of the allelic IgG2a to FcγRIV (Nimmerjahn et al., 2005).

As a result of these work efforts, integrity and binding affinity of recombinantly produced anti-MPO mAbs was ensured and enabled me to conduct studies on subclass-specific effects of anti-MPO mAbs *in vivo*.

5.2.2 Anti-MPO antibodies did not show an effect on neutrophils *in vitro*.

Several studies already analyzed the effect of patient sera or purified total ANCA on neutrophils to induce an oxidative burst (Falk et al., 1990, Pfister et al., 2004). PR3 as well as MPO ANCA triggered the generation of ROS, degranulation of neutrophils and the release of pro-inflammatory cytokines. To test the ability of the anti-MPO mAbs used in this study several assays including the measurement of neutrophil elastase released into the supernatant of treated neutrophils and superoxide dismutase-inhibitable reduction of ferricytochrome C were performed. Since none of these assays showed any activation of BM-isolated neutrophils, just one example for these negative results is given in Figure 8. Priming of BM-derived neutrophils with TNF-α and incubation with different anti-MPO mAbs as well as mAb combinations did not lead to increased amounts of DHR-positive cells comparable to the positive control. Unlike the neutrophils used in this project, extravasated neutrophils were used in other studies which were isolated from the peritoneal cavity after thioglycolate stimulation (Pfister et al., 2004). It might be objected, that naïve neutrophils derived from the bone-marrow of C57BL/6 mice were immature and not primed enough to be fully activated by mAbs.

Another potential concern explaining the negative outcome of this assay is that mAbs only bind to one distinct epitope on the surface of the antigen. As a consequence, crosslinking of multiple antigens and the triggering of FcγR signaling may be missing compared to polyclonal ANCA populations.

Recent investigations also showed that the activation of neutrophils by ANCA is not always observed (Popat and Robson, 2019). ANCA isolated from AAV patients were not able to induce degranulation and oxidative burst of neutrophils *in vitro*. This is in contrast to other studies

which report a significant activation of neutrophils with an induction of oxidative burst by purified anti-PR3 as well as anti-MPO ANCA (Franssen et al., 1999; Harper et al., 2001).

Based on these and our own observations, *in vitro* studies of anti-MPO and anti-PR3 antibodies to induce neutrophil activation have to be optimized in order to obtain reproducable and reliable results.

5.2.3 Pulmonary vasculitis can be induced subclass-specific with IgG2c anti-MPO

To investigate subclass-specific pathogenicity of anti-MPO mAbs *in vivo* we modified an experimental model of pulmonary vasculitis. The same combination of anti-MPO clones 6D1 and 6G4 was used with the difference that we applied both antibodies either in recombinant IgG1 or in IgG2c format. In addition, two control groups treated with the respective isotype control antibodies were included. Five days after the first mAb injection a pathogenic phenotype could be observed in mice treated with IgG2c anti-MPO. All other groups showed no or moderate phenotypes that can be mainly attributed to the intratracheal injection of LPS and fMLP as infectious trigger.

The most prominent observation indicating a pathogenic effect of IgG2c anti-MPO was the occurrence of pulmonary hemorrhages that were completely absent in other experimental groups. The observed hemorrhages (Figure 10) as well as measured infiltration of protein (Figure 11C) into the lungs of IgG2c-treated mice are marks of vascular capillaritis and therefore suggest a pathogenic role of IgG2c anti-MPO antibodies in pulmonary vasculitis *in vivo*.

Leucocytes are known to play key roles in the pathophysiology of AAV. Especially eosinophils are a hallmark of EGPA, a subtype of AAV which is characterized by the occurrence of anti-MPO ANCA. Referring the numbers of eosinophils to the total leucocyte numbers in the BALF samples, we noticed a highly increased ratio in the IgG2c-treated group (Figure 11B). To a lesser extend the ratio between neutrophils and total leucocytes was also found to be higher

in this group. These observations are in line with the occurrence of eosinophils and neutrophils in vascular and extravascular infiltrates in lungs and kidneys of AAV patients (Xiao et al., 2005). The histology of a healthy lung of untreated control animals is characterized by delicately thin alveolar septae with some moderate alterations which are due to the tracheal instillation of fixation solution. These artefacts include occasional vessel enlargement and their expansion by intravascular erythrocytes as well as focally expanded ruptures of alveolar septae. Rarely, free erythrocytes were detected in the alveolar lumina.

Mice treated with IgG2c anti-MPO showed histological alterations in the lung tissue that were morphologically compatible with a vascular damage experimentally induced by administration of fMLP, LPS and systemic application of mAbs directed against MPO. Lipopolysaccharide (LPS) is known to trigger a cascade in which neutrophils are recruited from the venules by interaction with selectins and integrins expressed by endothelial cells upon infection. Circulating neutrophils are captured by these molecules and roll along the vasculature where they finally adhere. Investigations by Yipp et al. (2017) reveal that this classical inflammatory cascade is not observed in the lung, where selectins and integrins appear to be not required for neutrophil recruitment to capillary vessels during inflammation. Instead neutrophils form resident interstitial reservoirs and clear lung-sequestered pathogens from the capillary circulation. The narrow diameter of the lung capillaries as well as the low blood pressure present in the pulmonary vasculature contribute to the retention of a large number of neutrophils. We indeed observed this recruitment and accumulation of neutrophils in lung capillaries of IgG2c anti-MPO-treated mice as shown in Figure 12A.

Variably severe alveolar hemorrhages present in lung tissue of IgG2c anti-MPO treated mice indicated an acute destruction of the vascular walls of small pulmonary vessels. Considering the experimental procedure and the observed alterations in lung sections, a pathogenesis mimicking an ANCA-mediated disease is plausible.

Performance of bronchoalveolar lavage before fixation of the lungs led to removal of inflammaroty cells from the bronchi and alveoli as determined by flow cytometry (Figures 10

and 11). The content of inflammatory cells in the examined lung tissue, thus, was reduced. Overall, the quality and extent of histopathological alterations were qualified as most severe in mice treated with IgG2c anti-MPO. In order to include additional histomorphological parameters, like the extent of granulocyte and macrophage infiltration, vascular integrity and extracellular matrix deposition, further histological and immunohistological examinations were performed. The results obtained in this way confirmed the pathology observed and anticipated by H&E staining. CD31 staining of endothelial cells revealed an accumulation of cells around the alveolar capillaries at inflammatory foci in the lungs of IgG2c-treated mice. Furthermore, predominance of Mac-2 positive macrophages within the inflammatory cell population could be observed. The involvement of eosinophils seems to exceed the number of neutrophils and confirms the previous histopathological assessment based on the evaluation of H&E-stained sections as determined by Giemsa staining. The lack of neutrophils in the lung tissues of all groups could have been caused by the lavage of the lungs prior to fixation of the tissue. The occurrence of eosinophils in the tissue is thus even more striking since a significant effect is also seen in the "washed out" BAL cell population.

Even though the morphological changes and histopathological alterations observed in the examined lung tissue were not entirely comparable to those of the different entities of pulmonary lesions displayed in human ANCA-vasculitis, the pathogenicity of IgG2c anti-MPO in pulmonary vasculitis can be specifically attributed to the subclass since epitope-matched IgG1 anti-MPO were not able to induce a similarly severe vasculitis-like phenotype.

5.2.4 Application of the results to human disease

Results obtained from immunological investigations in model organisms like mice must always been interpreted with caution and prudence and the awareness of significant species differences. Differences in the expression of target antigens as well as dissimilar existing IgG subclasses and FcγRs calls for caution in the translation of the results to human disease. According to the genetic locus as well as structural properties, the murine subclass IgG2c is

known to be the functional homologue of human IgG1. IgG2c has the highest affinity to interact with murine FcγRIV as well as its human homologue human FcγRIIIA. Since the polymorphic FcγRIIIA^{158V} has high affinity to human IgG1 and is furthermore associated with AAV, our results infer a role of this specific receptor for the pathogenesis of this disease. Therapeutic antibodies targeting FcγRIIIA and blocking the effector signaling could be applied in critical stages of the disease when patients show high plasma levels of IgG1 ANCA.

Unquestionably, deeper investigations need to be done in relation to subclass-specific effects of ANCA but this study shows for the first time *in vivo* that the subclasses of anti-MPO antibodies matters for the pathogenicity of ANCA in vasculitis.

5.2.5 Limitations of the study

As already mentioned, translation of results from mice to humans have to be interpreted with caution. General differences in the immune system like the homology of IgG subclasses and FcγRs increases the challenges for translatable interpretation. Furthermore, experimental animals are usually kept under specific pathogen-free conditions and thus have a completely different antibody repertoire compared to humans that are exposed to diverse foreign antigens constantly. The development of antibodies against these foreign proteins, even though they are not directed against autoantigens, changes the immune profile of each individual and has to be considered in the interpretation of *in vivo* results from mice.

Even though the observed phenotype cannot be specifically categorized as a single clinical entity of AAV, the overall effect is mimicking features of pulmonary vasculitis. In recent years the diagnosis and subgrouping of different clinical AAV entities has been controversially discussed (Deshayes et al., 2019; Mahr et al., 2019; Lamprecht et al., 2020). Classification based on the occurrence of ANCA and their specific target antigen has been proposed in order to predict the clinical outcome of AAV patients more accurately (Reviewed in Cornec et al., 2016). Based on the overlap in the disease symptoms and courses a phenotypic distinction between GPA, EGPA and MPA based on clinical and histological features has been

questioned. In view of this, the phenotype presented in this study can be classified generally as AAV-like.

5.2.6 Future plans

In order to address the mechanism behind the subclass-specific pathogenicity, the *in vivo* experiments should be repeated in transgenic mice deficient in specific FcγRs, first of all FcγRIV. Application of the vasculitis-inducing combination of IgG2c anti-MPO 6D1 and 6G4 to these receptor knockout mice could give insights into the signaling pathways involved. With this experimental setup also a potential activation of complement by IgG2c anti-MPO should be excluded.

It was furthermore shown, that glycosylation of antibodies plays a pivotal role in the induction of effector mechanisms via FcγR as well as the activation of complement (Kao et al., 2015). The authors show, that IgG2c, the murine subclass with the highest cytotoxic activity, was the only subclass which was still functional when it was minimally glycosylated with only mono- or disaccharide residues attached to the N297 glycosylation site. Complement, however, was not activated anymore after exposure to EndoS, which removed the majority of N-linked carbohydrates. Complete removal of the glycan by PNGase F eventually also abrogated the effect of IgG2c in the induction of cytotoxicity and resulted in an effector-less antibody. The same effects were observed also for human antibodies of the IgG1 and IgG3 subclasses, the main subclasses involved in cytotoxic antibody activity in humans. Application of our mAbs treated either with EndoS or PNGase F could therefore give additional insight into the mechanistic action in the *in vivo* setup.

For the suggested experiments, high amounts of recombinant mAbs would have to be provided. With an average yield of 5 µg per mL of transfected HEK293EBNA cell culture, high quantities of transfections were needed for this study. To reduce the workload, attempts to increase the yield of recombinant mAbs should be made. Co-transfection of the 10-fold amount of empty vector was shown to be sufficient for this study, but further dilution of the transfected

mAb plasmids and supplementation of empty vector could be tested for higher efficacy. Other methods like the co-transfection of low concentrations of valproic acid have also been shown to greatly increase the production of recombinant proteins in HEK293EBNA cells (Backliwal et al. 2008).

5.2.7 General conclusion

In this thesis I could show for the first time *in vivo* that the subclass of ANCA might play a role in the pathogenesis of AAV. Functional antibodies of different subclasses were produced recombinantly, characterized, and applied in a model of pulmonary vasculitis. *In vivo* data presented in this study show that systemic application of recombinant anti-MPO IgG2c caused a vasculitis-like phenotype with hemorrhages and inflammation in the lungs of mice, while the epitope-matched recombinant IgG1 antibody had no effect in this experimental pulmonary model. These findings indicate a crucial effect of subclass-specific antibody pathogenicity in pulmonary vasculitis in mice and suggest a potential similar mechanism in humans.

6. References

Aasarød K, Iversen BM, Hammerstrøm J, Bostad L, Vatten L, Jørstad S. Wegener's granulomatosis: clinical course in 108 patients with renal involvement. Nephrol Dial Transplant. 2000, 15 (5), 611-8. Erratum in: Nephrol Dial Transplant 2000, 15 (12), 2069.

Arnold JN, Wormald MR, Sim RB, Rudd PM, Dwek RA. The impact of glycosylation on the biological function and structure of human immunoglobulins. Annu Rev Immunol. 2007, 25, 21-50. Review.

Backliwal G, Hildinger M, Kuettel I, Delegrange F, Hacker DL, Wurm FM. Valproic acid: a viable alternative to sodium butyrate for enhancing protein expression in mammalian cell cultures. Biotechnol Bioeng. 2008, 101(1), 182-9.

Berti A, Cornec D, Crowson CS, Specks U, Matteson EL. The Epidemiology of Antineutrophil Cytoplasmic Autoantibody-Associated Vasculitis in Olmsted County, Minnesota: A Twenty-Year US Population-Based Study. Arthritis Rheumatol. 2017, (12), 2338-2350.

Bowden TA, Baruah K, Coles CH, Harvey DJ, Yu X, Song BD, Stuart DI, Aricescu AR, Scanlan CN, Jones EY, Crispin M. Chemical and structural analysis of an antibody folding intermediate trapped during glycan biosynthesis. J Am Chem Soc. 2012, 134 (42), 17554-63.

Brouwer E, Tervaert JW, Horst G, Huitema MG, van der Giessen M, Limburg PC, Kallenberg CG. Predominance of IgG1 and IgG4 subclasses of anti-neutrophil cytoplasmic autoantibodies (ANCA) in patients with Wegener's granulomatosis and clinically related disorders. Clin Exp Immunol. 1991, 83 (3), 379-86.

Bruhns P, Iannascoli B, England P, Mancardi DA, Fernandez N, Jorieux S, Daëron M. Specificity and affinity of human Fcgamma receptors and their polymorphic variants for human IgG subclasses. Blood. 2009, 113 (16), 3716-25.

Bruhns P. Properties of mouse and human IgG receptors and their contribution to disease models. Blood. 2012, 119 (24), 5640-9.

Bruhns P, Jönsson F. Mouse and human FcR effector functions. Immunol Rev. 2015, 268 (1), 25-51.

Bujak E, Matasci M, Neri D, Wulhfard S. Reformatting of scFv antibodies into the scFv-Fc format and their downstream purification. Methods Mol Biol. 2014, 1131, 315-34.

Burton DR. Immunoglobulin G: functional sites. Mol Immunol. 1985, 22 (3), 161-206. Review.

Carmona-Rivera C, Kaplan MJ. Low-density granulocytes: a distinct class of neutrophils in systemic autoimmunity. Semin Immunopathol. 2013, 35 (4), 455-63.

Cartin-Ceba R, Indrakanti D, Specks U, Stone JH, Hoffman GS, Kallenberg CG, Langford CA, Merkel PA, Spiera RF, Monach PA, St Clair EW, Seo P, Tchao NK, Ytterberg SR, Brunetta PG, Song H, Birmingham D, Rovin BH; RAVE-Immune Tolerance Network Research Group. The pharmacogenomic association of Fcγ receptors and cytochrome P450 enzymes with response to rituximab or cyclophosphamide treatment in antineutrophil cytoplasmic antibody-associated vasculitis. Arthritis Rheumatol. 2017, 69 (1), 169-175.

Colman R, Hussain A, Goodall M, Young SP, Pankhurst T, Lu X, Jefferis R, Savage CO, Williams JM. Chimeric antibodies to proteinase 3 of IgG1 and IgG3 subclasses induce different magnitudes of functional responses in neutrophils. Ann Rheum Dis. 2007, 66 (5), 676-82.

Cornec D, Cornec-Le Gall E, Fervenza FC, Specks U. ANCA-associated vasculitis - clinical utility of using ANCA specificity to classify patients. Nat Rev Rheumatol. 2016, 12 (10), 570-9.

Cornec D, Kabat BF, Mills JR, Cheu M, Hummel AM, Schroeder DR, Cascino MD, Brunetta P, Murray DL, Snyder MR, Fervenza F, Hoffman GS, Kallenberg CGM, Langford CA, Merkel PA, Monach PA, Seo P, Spiera RF, St Clair EW, Stone JH, Barnidge DR, Specks U. Pharmacokinetics of rituximab and clinical outcomes in patients with anti-neutrophil cytoplasmic antibody associated vasculitis. Rheumatology (Oxford). 2018, 57 (4), 639-650.

Daëron M, Jaeger S, Du Pasquier L, Vivier E. Immunoreceptor tyrosine-based inhibition motifs: a quest in the past and future. Immunol Rev. 2008, 224, 11-43.

Dangl JL, Wensel TG, Morrison SL, Stryer L, Herzenberg LA, Oi VT. Segmental flexibility and complement fixation of genetically engineered chimeric human, rabbit and mouse antibodies. EMBO J. 1988, 7 (7), 1989-94.

Davies DJ, Moran JE, Niall JF, Ryan GB. Segmental necrotizing glomerulonephritis with antineutrophil antibody: possible arbovirus aetiology? Br Med J (Clin Res Ed). 1982, 285, 606.

Deshayes S, Martin Silva N, Khoy K, Yameogo S, Mariotte D, Lobbedez T, Aouba A. Clinical impact of subgrouping ANCA-associated vasculitis according to antibody specificity beyond the clinicopathological classification. Rheumatology (Oxford). 2019, 58 (10), 1731-1739.

Drooger JC, Dees A, Swaak AJ. ANCA-Positive Patients: The Influence of PR3 and MPO Antibodies on Survival Rate and The Association with Clinical and Laboratory Characteristics. Open Rheumatol J. 2009, 3, 14-17.

Ewert BH, Jennette JC. Falk, RJ. Anti-myeloperoxidase antibodies stimulate neutrophils to damage human endothelial cells. Kidney Int 1992, 41 (2), 375-83.

Falk RJ, Jennette JC. Anti-neutrophil cytoplasmic autoantibodies with specificity for myeloperoxidase in patients with systemic vasculitis and idiopathic necrotizing and crescentic glomerulonephritis. N Engl J Med. 1988, 318 (25),1651-7.

Falk RJ, Terrell RS, Charles LA, Jennette JC. Anti-neutrophil cytoplasmic autoantibodies induce neutrophils to degranulate and produce oxygen radicals *in vitro*. Proc Natl Acad Sci U S A 1990, 87 (11), 4115-9.

Fauci AS, Wolff SM. Wegener's granulomatosis: studies in eighteen patients and a review of the literature. 1973. Medicine (Baltimore). 1994, 73 (6), 315-24.

Flossmann O, Berden A, de Groot K, Hagen C, Harper L, Heijl C, Höglund P, Jayne D, Luqmani R, Mahr A, Mukhtyar C, Pusey C, Rasmussen N, Stegeman C, Walsh M, Westman K; European Vasculitis Study Group. Long-term patient survival in ANCA-associated vasculitis. Ann Rheum Dis. 2011, 70 (3), 488-94.

Franssen CF, Huitema MG, Muller Kobold AC, Oost-Kort WW, Limburg PC, Tiebosch A, Stegeman CA, Kallenberg CG, Tervaert JW. *In vitro* neutrophil activation by antibodies to proteinase 3 and myeloperoxidase from patients with crescentic glomerulonephritis. J Am Soc Nephrol. 1999, 10 (7), 1506-15.

Fries JF, Hunder GG, Bloch DA, Michel BA, Arend WP, Calabrese LH, Fauci AS, Leavitt RY, Lie JT, Lightfoot RW Jr, et al. The American College of Rheumatology 1990 criteria for the classification of vasculitis. Summary. Arthritis Rheum. 1990, 33 (8), 1135-6.

Frohnert PP, Sheps SG. Long-term follow-up study of periarteritis nodosa. Am J Med 1967, 43 (1), 8-14.

Gioffredi A, Maritati F, Oliva E, Buzio C. Eosinophilic granulomatosis with polyangiitis: an overview. Front Immunol. 2014, 5, 549.

Hagen EC, Daha MR, Hermans J, Andrassy K, Csernok E, Gaskin G, Lesavre P, Lüdemann J, Rasmussen N, Sinico RA, Wiik A, van der Woude FJ. Diagnostic value of standardized assays for anti-neutrophil cytoplasmic antibodies in idiopathic systemic vasculitis. EC/BCR Project for ANCA Assay Standardization. Kidney Int. 1998, 53 (3), 743-53.

Halbwachs-Mecarelli L, Bessou G, Lesavre P, Lopez S, Witko-Sarsat V. Bimodal distribution of proteinase 3 (PR3) surface expression reflects a constitutive heterogeneity in the polymorphonuclear neutrophil pool. FEBS Lett. 1995, 374 (1), 29-33.

Harper L, Radford D, Plant T, Drayson M, Adu D, Savage CO. IgG from myeloperoxidase-antineutrophil cytoplasmic antibody-positive patients stimulates greater activation of primed neutrophils than IgG from proteinase 3-antineutrophil cytosplasmic antibody-positive patients. Arthritis Rheum. 2001, 44 (4), 921-30.

Hartl DM, Aïdan P, Brugière O, Sterkers O. Wegener's granulomatosis presenting as a recurrence of chronic otitis media. Am J Otolaryngol. 1998, 19 (1), 54-60.

Hewins P, Morgan MD, Holden N, Neil D, Williams JM, Savage CO, Harper L. IL-18 is upregulated in the kidney and primes neutrophil responsiveness in ANCA-associated vasculitis. Kidney Int. 2006, 69 (3), 605-15.

Hilhorst M, van Paassen P, Tervaert JW; Limburg Renal Registry. Proteinase 3-ANCA Vasculitis versus Myeloperoxidase-ANCA Vasculitis. J Am Soc Nephrol. 2015, 26 (10), 2314-27.

Hoffman GS, Kerr GS, Leavitt RY, Hallahan CW, Lebovics RS, Travis WD, Rottem M, Fauci AS. Wegener granulomatosis: an analysis of 158 patients. Ann Intern Med. 1992, 116 (6), 488-98.

Huugen, D. (2007). Myeloperoxidase and anti-myeloperoxidase autoantibodies in renal inflammation. Maastricht: Universiteit Maastricht. Dissertation.

Janeway CA Jr, Travers P, Walport M, et al. Immunobiology: The Immune System in Health and Disease. 5th edition. New York: Garland Science; 2001.

Jennette JC, Wilkman AS, Falk RJ. Diagnostic predictive value of ANCA serology. Kidney Int 1998, 53 (3), 796-8.

Jennette JC, Falk RJ, Bacon PA, Basu N, Cid MC, Ferrario F, Flores-Suarez LF, Gross WL, Guillevin L, Hagen EC, Hoffman GS, Jayne DR, Kallenberg CG, Lamprecht P, Langford CA, Luqmani RA, Mahr AD, Matteson EL, Merkel PA, Ozen S, Pusey CD, Rasmussen N, Rees AJ, Scott DG, Specks U, Stone JH, Takahashi K, Watts RA. 2012 revised International Chapel Hill Consensus Conference Nomenclature of Vasculitides. Arthritis Rheum. 2013, 65 (1), 1-11.

Kabat EA, Wu TT, Bilofsky H. Variable region genes for the immunoglobulin framework are assembled from small segments of DNA-a hypothesis. Proc Natl Acad Sci U S A. 1978, 75 (5), 2429-33.

Jerke U, Rolle S, Dittmar G, Bayat B, Santoso S, Sporbert A, Luft F, Kettritz R. Complement receptor Mac-1 is an adaptor for NB1 (CD177)-mediated PR3-ANCA neutrophil activation. J Biol Chem. 2011, 286 (9), 7070-81.

Kao D, Danzer H, Collin M, Groß A, Eichler J, Stambuk J, Lauc G, Lux A, Nimmerjahn F. A Monosaccharide Residue Is Sufficient to Maintain Mouse and Human IgG Subclass Activity and Directs IgG Effector Functions to Cellular Fc Receptors. Cell Rep. 2015, 22, 13 (11), 2376-2385.

Kaplon H, Muralidharan M, Schneider Z, Reichert JM. Antibodies to watch in 2020. MAbs. 2020, 12 (1),1703531.

Katsuyama T, Sada KE, Makino H. Current concept and epidemiology of systemic vasculitides. Allergol Int. 2014, 63 (4), 505-13.

Kessenbrock K, Krumbholz M, Schönermarck U, Back W, Gross WL, Werb Z, Gröne HJ, Brinkmann V, Jenne DE. Netting neutrophils in autoimmune small-vessel vasculitis. Nat Med. 2009, 15 (6), 623-5.

Kettritz R. How anti-neutrophil cytoplasmic autoantibodies activate neutrophils. Clin Exp Immunol 2012, 169 (3), 220-8.

Korkmaz B, Kuhl A, Bayat B, Santoso S, Jenne DE. A hydrophobic patch on proteinase 3, the target of autoantibodies in Wegener granulomatosis, mediates membrane binding via NB1 receptors. J Biol Chem. 2008, 283 (51), 35976-82.

Lamprecht P, Müller A, Witko-Sarsat V, Guillevin L. Comment on: Subclassifying ANCA-associated vasculitis: a unifying view of disease spectrum. Rheumatology (Oxford). 2020 Mar 12.

Lanham JG, Elkon KB, Pusey CD, Hughes GR. Systemic vasculitis with asthma and eosinophilia: a clinical approach to the Churg-Strauss syndrome. Medicine (Baltimore). 1984, 63 (2), 65-81.

Li Z, Woo CJ, Iglesias-Ussel MD, Ronai D, Scharff MD. The generation of antibody diversity through somatic hypermutation and class switch recombination. Genes Dev 2004, 18 (1), 1-11.

Lieber M. Antibody diversity: a link between switching and hypermutation. Curr Biol 2000, 10 (21), R798-800.

Liu H, May K. Disulfide bond structures of IgG molecules: structural variations, chemical modifications and possible impacts to stability and biological function. MAbs. 2012 Jan, 4 (1), 17-23.

Lu X, Garfield A, Rainger GE, Savage CO, Nash GB. Mediation of endothelial cell damage by serine proteases, but not superoxide, released from antineutrophil cytoplasmic antibody-stimulated neutrophils. Arthritis Rheum 2006, 54 (5), 1619-28.

Mahr A, Moosig F, Neumann T, Szczeklik W, Taillé C, Vaglio A, Zwerina J. Eosinophilic granulomatosis with polyangiitis (Churg-Strauss): evolutions in classification, etiopathogenesis, assessment and management. Curr Opin Rheumatol. 2014, 26 (1), 16-23.

Mahr A, Specks U, Jayne D. Subclassifying ANCA-associated vasculitis: a unifying view of disease spectrum. Rheumatology (Oxford). 2019, 58 (10), 1707-1709.

Mechetina LV, Najakshin AM, Alabyev BY, Chikaev NA, Taranin AV. Identification of CD16-2, a novel mouse receptor homologous to CD16/Fc gamma RIII. Immunogenetics. 2002, 54 (7), 463-8.

Mellbye OJ, Mollnes TE, Steen LS. IgG subclass distribution and complement activation ability of autoantibodies to neutrophil cytoplasmic antigens (ANCA). Clin Immunol Immunopathol. 1994, 70 (1), 32-9.

Merkel PA, Polisson RP, Chang Y, Skates SJ, Niles JL. Prevalence of antineutrophil cytoplasmic antibodies in a large inception cohort of patients with connective tissue disease. Ann Intern Med 1997, 126 (11), 866-73.

Mulder AH, Stegeman CA, Kallenberg CG. Activation of granulocytes by anti-neutrophil cytoplasmic antibodies (ANCA) in Wegener's granulomatosis: a predominant role for the IgG3 subclass of ANCA. Clin Exp Immunol. 1995, 101 (2), 227-32.

Nelson AL. Antibody fragments: hope and hype. MAbs. 2010, 2 (1), 77–83.

Nimmerjahn F, Bruhns P, Horiuchi K, Ravetch JV. FcgammaRIV: a novel FcR with distinct IgG subclass specificity. Immunity. 2005, 23 (1), 41-51.

Nimmerjahn F, Ravetch JV. Fcgamma receptors: old friends and new family members. Immunity. 2006, 24 (1), 19-28.
Nimmerjahn F. Activating and inhibitory FcgammaRs in autoimmune disorders. Springer Semin Immunopathol 2006, 28 (4), 305-19

Noll S, Schaub-Kuhnen, S. Praxis der Immunhistochemie: Herausgegeben von Heinz Höfler und Klaus-Michael Müller (Deutsch) Gebundenes Buch – 19. Oktober 2000

Ntatsaki E, Watts RA, Scott DG. Epidemiology of ANCA-associated vasculitis. Rheum Dis Clin North Am. 2010, 36 (3), 447-61.

Ono N, Inoue Y, Miyamura T, Ueda N, Nagano S, Inoue H, Oryoji K, Ota SI, Sawabe T, Yoshizawa S, Takeyama Y, Sadanaga Y, Takamori A, Kimoto Y, Miyake K, Horiuchi T, Nakashima H, Niiro H, Tada Y. The association of airway comorbidities with the clinical phenotypes and outcomes of ANCA-associated vasculitis patients. J Rheumatol. 2019.

Ortiz DF, Lansing JC, Rutitzky L, Kurtagic E, Prod'homme T, Choudhury A, Washburn N, Bhatnagar N, Beneduce C, Holte K, Prenovitz R, Child M, Killough J, Tyler S, Brown J, Nguyen S, Schwab I, Hains M, Meccariello R, Markowitz L, Wang J, Zouaoui R, Simpson A, Schultes B, Capila I, Ling L, Nimmerjahn F, Manning AM, Bosques CJ. Elucidating the interplay between IgG-Fc valency and FcγR activation for the design of immune complex inhibitors. Sci Transl Med. 2016, 8 (365), 365ra158.

Pfister H, Ollert M, Fröhlich LF, Quintanilla-Martinez L, Colby TV, Specks U, Jenne DE. Antineutrophil cytoplasmic autoantibodies against the murine homolog of proteinase 3 (Wegener autoantigen) are pathogenic *in vivo*. Blood. 2004, 104 (5), 1411-8.

Popat RJ, Robson MG. Neutrophils are not consistently activated by antineutrophil cytoplasmic antibodies *in vitro*. Ann Rheum Dis. 2019, 78 (5), 709-711.

Ra C, Jouvin MH, Blank U, Kinet JP. A macrophage Fc gamma receptor and the mast cell receptor for IgE share an identical subunit. Nature. 1989, 341 (6244), 752-4.

Ravetch JV, Perussia B. Alternative membrane forms of Fc gamma RIII(CD16) on human natural killer cells and neutrophils. Cell type-specific expression of two genes that differ in single nucleotide substitutions. J Exp Med. 1989, 170 (2), 481-97.

Reff ME, Carner K, Chambers KS, Chinn PC, Leonard JE, Raab R, Newman RA, Hanna N, Anderson DR., Depletion of B cells *in vivo* by a chimeric mouse human monoclonal antibody to CD20. Blood 1994, 83 (2), 435-45.

Reth M. Antigen receptor tail clue. Nature. 1989, 338 (6214), 383-4.

Robledo G, Márquez A, Dávila-Fajardo CL, Ortego-Centeno N, Rubio JL, Garrido Ede R, Sánchez-Román J, García-Hernández FJ, Ríos-Fernández R, González-Escribano MF, García MT, Palma MJ, Ayala Mdel M, Martín J. Association of the FCGR3A-158F/V gene polymorphism with the response to rituximab treatment in Spanish systemic autoimmune disease patients. DNA Cell Biol. 2012, 31(12), 1671-7.

Romeis: Mikroskopische Technik. M. Mulisch, U. Welsch (Hrsg.). 19., überarb. u. erw. Auflage 2015, Hardcover.

Roux KH, Strelets L, Michaelsen TE. Flexibility of human IgG subclasses. J Immunol. 1997, 159 (7), 3372-82.

Rutgers A, Heeringa P, Damoiseaux JG, Tervaert JW. ANCA and anti-GBM antibodies in diagnosis and follow-up of vasculitic disease. Eur J Intern Med 2003, 14 (5), 287-295.

Sablé-Fourtassou R, Cohen P, Mahr A, Pagnoux C, Mouthon L, Jayne D, Blockmans D, Cordier JF, Delaval P, Puechal X, Lauque D, Viallard JF, Zoulim A, Guillevin L; French Vasculitis Study Group. Antineutrophil cytoplasmic antibodies and the Churg-Strauss syndrome. Ann Intern Med. 2005, 143 (9), 632-8.

Scallon BJ, Scigliano E, Freedman VH, Miedel MC, Pan YC, Unkeless JC, Kochan JP. A human immunoglobulin G receptor exists in both polypeptide-anchored and phosphatidylinositol-glycan-anchored forms. Proc Natl Acad Sci U S A. 1989, 86 (13), 5079-83.

Schreiber A, Eulenberg-Gustavus C, Bergmann A, Jerke U, Kettritz R. Lessons from a double-transgenic neutrophil approach to induce antiproteinase 3 antibody-mediated vasculitis in mice. J Leukoc Biol 2016, 100 (6), 1443-1452.

Schur PH. IgG subclasses. A historical perspective. Monogr Allergy. 1988, 23, 1-11
Scully C, Langdon J, Evans J. Marathon of eponyms: 23 Wegener granulomatosis. Oral Dis. 2012, 18 (2), 214-6.

Sengelov H, Follin P, Kjeldsen L, Lollike K, Dahlgren C, Borregaard N. Mobilization of granules and secretory vesicles during *in vivo* exudation of human neutrophils. J Immunol 1995, 154 (8), 4157-65.

Sinico RA, Di Toma L, Maggiore U, Bottero P, Radice A, Tosoni C, Grasselli C, Pavone L, Gregorini G, Monti S, Frassi M, Vecchio F, Corace C, Venegoni E, Buzio C. Prevalence and clinical significance of antineutrophil cytoplasmic antibodies in Churg-Strauss syndrome. Arthritis Rheum. 2005, 52 (9), 2926-35.

Sondermann P, Huber R, Oosthuizen V, Jacob U. The 3.2-A crystal structure of the human IgG1 Fc fragment-Fc gammaRIII complex. Nature. 2000, 406 (6793), 267-73.

Stegeman CA, Tervaert JW, Sluiter WJ, Manson WL, de Jong PE, Kallenberg CG. Association of chronic nasal carriage of Staphylococcus aureus and higher relapse rates in Wegener granulomatosis. Ann Intern Med. 1994,120 (1),12-7.

Torres M, Fernández-Fuentes N, Fiser A, Casadevall A. The immunoglobulin heavy chain constant region affects kinetic and thermodynamic parameters of antibody variable region interactions with antigen. J Biol Chem. 2007, 282 (18), 13917-27.

Ui Mhaonaigh A, Coughlan AM, Dwivedi A, Hartnett J, Cabral J, Moran B, Brennan K, Doyle SL, Hughes K, Lucey R, Floudas A, Fearon U, McGrath S, Cormican S, De Bhailis A, Molloy

EJ, Brady G, Little MA. Low Density Granulocytes in ANCA Vasculitis Are Heterogenous and Hypo-Responsive to Anti-Myeloperoxidase Antibodies. Front Immunol. 2019, 10, 2603.

van der Woude FJ, Rasmussen N, Lobatto S, Wiik A, Permin H, van Es LA, van der Giessen M, van der Hem GK, The TH. Autoantibodies against neutrophils and monocytes: tool for diagnosis and marker of disease activity in Wegener's granulomatosis. Lancet. 1985, 1 (8426), 425-9.

van Timmeren MM, van der Veen BS, Stegeman CA, Petersen AH, Hellmark T, Collin M, Heeringa P. IgG glycan hydrolysis attenuates ANCA-mediated glomerulonephritis. J Am Soc Nephrol. 2010, 21 (7), 1103-14.

Vega LE, Espinoza LR. Predictors of Poor Outcome in ANCA-Associated Vasculitis (AAV). Curr Rheumatol Rep 2016, 18 (12), 70.

Warmerdam PA, van de Winkel JG, Gosselin EJ, Capel PJ. Molecular basis for a polymorphism of human Fc gamma receptor II (CD32). J Exp Med. 1990, 172 (1), 19-25.

Watts RA, Lane SE, Bentham G, Scott DG. Epidemiology of systemic vasculitis: a ten-year study in the United Kingdom. Arthritis Rheum. 2000, 43 (2), 414-9.

Watts RA, Mahr A, Mohammad AJ, Gatenby P, Basu N, Flores-Suarez LF. Classification, epidemiology and clinical subgrouping of antineutrophil cytoplasmic antibody (ANCA)-associated vasculitis. Nephrol Dial Transplant 2015, 30 (Suppl 1), i14-22.

Weber SS, Ducry J, Oxenius A. Dissecting the contribution of IgG subclasses in restricting airway infection with *Legionella pneumophila*. J Immunol. 2014, 193 (8), 4053-9.

Xiao H, Heeringa P, Hu P, Liu Z, Zhao M, Aratani Y, Maeda N, Falk RJ, Jennette JC. Antineutrophil cytoplasmic autoantibodies specific for myeloperoxidase cause glomerulonephritis and vasculitis in mice. J Clin Invest. 2002, 110 (7), 955-63.

Xiao H, Heeringa P, Liu Z, Huugen D, Hu P, Maeda N, Falk RJ, Jennette JC. The role of neutrophils in the induction of glomerulonephritis by anti-myeloperoxidase antibodies. Am J Pathol. 2005, 167 (1), 39-45.

Yipp BG, Kim JH, Lima R, Zbytnuik LD, Petri B, Swanlund N, Ho M, Szeto VG, Tak T, Koenderman L, Pickkers P, Tool ATJ, Kuijpers TW, van den Berg TK, Looney MR, Krummel MF, Kubes P. The Lung is a Host Defense Niche for Immediate Neutrophil-Mediated Vascular Protection. Sci Immunol. 2017, 28, 2 (10).

Zauner G, Selman MH, Bondt A, Rombouts Y, Blank D, Deelder AM, Wuhrer M. Glycoproteomic analysis of antibodies. Mol Cell Proteomics. 2013, 12 (4), 856-65.

Zhang Z, Goldschmidt T, Salter H. Possible allelic structure of IgG2a and IgG2c in mice. Mol Immunol 2012, 50 (3), 169-71.

7. Abbreviations

AAV	ANCA-associated vasculitis
ANCA	Anti-neutrophil cytoplasmic antibody
BAL	Bronchoalveolar lavage
BALF	BAL fluid
BM	Bone marrow
bp	Base pair
BSA	Bovine serum albumin
C_H	Constant heavy chain region
C_L	Constant light chain region
DAH	Diffuse alveolar hemorrhage
dH_2O	Deionized water
DHR	Dihydrorhodamine 123
DNA	Deoxyribonucleic acid
EGPA	Eosinophilic granulomatosis with polyangiitis
ELISA	Enzyme-linked immunosorbent assay
EndoS	Endoglycosidase S
FACS	Fluorescence-activated cell scanning
Fc	Cristallizable fragment
FcγR	Cristallizable fragment gamma receptor
FFPE	Formalin-fixed paraffin embedded
fMLP	Formyl-methionyl-leucyl-phenylalanine
GPA	Granulomatosis with polyangiitis
H&E	Hematoxylin and eosin
HEK	Human embryonic kidney

His	Histidine
HRP	Horseradish peroxidase
IgG	Immunoglobulin G
I. p.	Intra peritoneal
I.t.	Intratracheal
kDa	Kilodalton
LB	Lysogeny broth
LPS	Lipopolysaccharide
mAb	Monoclonal antibody
MPA	Microscopic polyangiitis
MPO	Myeloperoxidase
mRNA	Messenger ribonucleic acid
MW	Molecular weight
NΦ	Neutrophil
NET	Neutrophil extracellular trap
NSP	Neutrophil serine protease
OD	Optical density
O.n.	Overnight
PBS	Phosphate buffered saline
PCR	Polymerase chain reaction
PEI	Polyethyleneimine
PMA	Phorbol-12-myristat-13-acetat
PMN	Polymorphonuclear cells
PNGase F	Peptide-N-Glycosidase F
PR3	Proteinase 3
PVDF	Polyvinylidene difluoride
ROS	Reactive oxygen species

RT	Room temperature
scFv-Fc	single chain variable fragment-constant fragment
TMB	3,3′,5,5′-Tetramethylbenzidin
TNF-α	Tumor necrosis factor alpha
V_H	Variable heavy chain region
V_L	Variable light chain region
WT	Wild type

8. Appendix

8.1 Presentations on national and international meetings

8.1.1 Oral presentations

“A major pathogenic role of the murine IgG2 subclass in experimental autoantibody-mediated vasculitis”. 5th general assembly meeting RELENT. Nice, France, 2019

“A major pathogenic role of the murine IgG2 subclass in experimental autoantibody-mediated vasculitis”. 36th Winter School on Proteinases and Their Inhibitors. Tiers, Italy, 2019

“Recombinant production and usage of monoclonal antibodies against target antigens in ANCA-associated vasculitides”. 4th general assembly meeting RELENT. Ramsau, Austria, 2019.

“Recombinant production and use of single-chain and two-chain antibodies to human PR3”. 34th Winter School on Proteinases and Their Inhibitors. Italy, 2017

8.1.2 Poster presentation

“A major pathogenic role of the murine IgG2 subclass in experimental autoantibody-mediated vasculitis”. DZL (Deutsches Zentrum für Lungenforschung) annual meeting. Travemünde, Germany, 2020

8.2 Acknowledgements

First, I would like to express my gratitude to my supervisor **PD Dr. Dieter Jenne**. Thank you for your support and all the hours of scientific discussions. You encouraged me to develop new ideas and to critically and independently approach problems and to solve them.
I sincerely respect your broad (and as I sometimes felt, unlimited) knowledge and I learned a lot, most importantly to be a scientist!

I also want to thank my supervisor at the faculty of biology, **Prof. Dr. Elisabeth Weiß**, for her support and supervision. I highly appreciate your interest and advice and I want to thank you especially for your support in these last, extraordinary and difficult, weeks.

Many thanks go to all our collaboration partners that contributed to this work, most of all to **Susanne Viehmann**. Without her support in performing the *in vivo* experiments, this work would not be as it is.

I am also thankful to **Dr. Ulf Schönermarck** who gave me interesting insights to the “other side” and added valuable suggestions to my project as part of my thesis advisory committee.

I want to acknowledge the financial support by the European Union’s H2020-PHC-2015 program **RELENT** (668036).

I had great pleasure of working with all the fantasic colleagues of the Jenne Lab.
Thank you for the cheerful and amicable working atmosphere!
Special thank goes to my colleague and friend **Salome Rehm** who accompanied me through the whole time and made it an unforgettable experience!

I also benefited greatly from my fellow PhD students and colleagues. Most of all I want to thank **Aurelia**, **Georgios**, **Anne-Sophie**, **Mario** and **Simon** for their friendship, advice and great times.

Finally, I am deeply grateful to **MY FAMILY** in Munich and Neumünster. Without your love, support and patience, this thesis would not have been possible.
Thank you!

8.3 Eidesstattliche Erklärung

Ich versichere hiermit an Eides statt, dass meine Dissertation selbständig und ohne unerlaubte Hilfsmittel angefertigt worden ist.

Die vorliegende Dissertation wurde weder ganz, noch teilweise bei einer anderen Prüfungskommission vorgelegt.

Ich habe noch zu keinem früheren Zeitpunkt versucht, eine Dissertation einzureichen oder an einer Doktorprüfung teilzunehmen.

München, den 28. April 2020 .....

Stefanie Anne Weiß